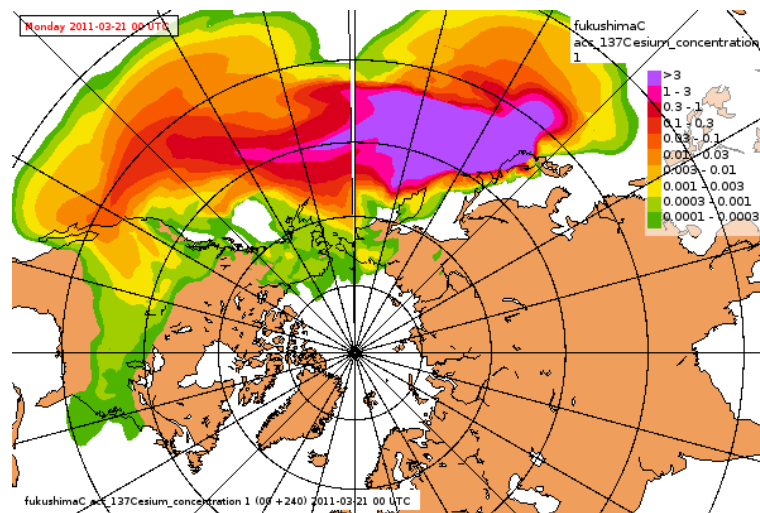


Report no. 4/2014  
Air Pollution  
ISSN: 0332-9879  
Oslo, January 31, 2014

# Development of the EEMEP model for applications in the ARGOS system

Heiko Klein and Jerzy Bartnicki







<b>Number</b> 4/2014	<b>Subject</b> Air Pollution	<b>Date</b> January 31, 2014	<b>Classification</b> <input checked="" type="checkbox"/> Open <input type="checkbox"/> Restricted <input type="checkbox"/> Confidential	<b>ISSN</b> 0332-9879
-------------------------	---------------------------------	---------------------------------	---	--------------------------

**Title**

Development of the EEMEP model for applications in the ARGOS system

**Authors**

Heiko Klein and Jerzy Bartnicki

**Client(s)**

Norwegian Radiation Protection Authority

**Client reference**

**Abstract**

This study has been performed by the scientists of the Norwegian Meteorological Institute (MET) for the Norwegian Radiation Protection Authority (NRPA) in the framework of EU project PREPARE. The main task of the study was a development and modification of the Eulerian dispersion model EEMEP, having in mind its future applications in the ARGOS system operating at NRPA. Here, we describe a preliminary version of the EEMEP model and its application for simulating atmospheric dispersion of radioactive debris for long lasting accident. We also present the results of preliminary comparison of the model results and limited number of measurements available for Fukushima accident. Finally the future interface between the EEMEP model at MET and the ARGOS at NRPA is discussed.

**Keywords**

Nuclear accident, risk assessment, atmospheric dispersion, radioactivity, emergency

**Disiplinary signature**

**Responsible signature**

\_\_\_\_\_

Hilde Fagerli

\_\_\_\_\_

Øystein Hov



# Contents

<b>1. Introduction</b>	<b>3</b>
<b>2. Eulerian EEMEP Model</b>	<b>7</b>
2.1. Model equations . . . . .	7
2.1.1. Continuity equation . . . . .	7
2.1.2. Advection . . . . .	7
2.1.3. Vertical diffusion . . . . .	8
2.1.4. Convection . . . . .	8
2.1.5. Source term for nuclear accident . . . . .	8
2.1.6. Source term for nuclear detonation . . . . .	9
2.1.7. Dry deposition . . . . .	10
2.1.8. Wet deposition . . . . .	11
2.1.9. Radioactive decay . . . . .	12
2.2. Operational applications of EEMEP model . . . . .	13
2.2.1. Operational set-up . . . . .	13
2.2.2. Nuclear accidents . . . . .	13
2.2.3. Nuclear explosions . . . . .	13
2.2.4. On demand simulations . . . . .	14
2.3. Results of the operational EEMEP model . . . . .	14
2.3.1. Results for nuclear accidents . . . . .	14
2.3.2. Results for nuclear explosions . . . . .	20
<b>3. Model simulation for long term release</b>	<b>21</b>
3.1. Source term for long release . . . . .	21
3.1.1. Source term with constant emissions . . . . .	21
3.1.2. Source term with variable emissions . . . . .	21
3.2. Model results for long release simulations . . . . .	21
3.2.1. Results for the release with constant emissions . . . . .	22
3.2.2. Results for the release with variable emissions . . . . .	23
<b>4. Preliminary comparison of model results with measurements</b>	<b>25</b>
<b>5. Model results in the ARGOS system</b>	<b>30</b>
5.1. Computational scheme for nuclear accident . . . . .	30
5.2. An example of remote application for nuclear accident . . . . .	32
<b>6. Conclusions</b>	<b>35</b>
<b>References</b>	<b>37</b>
<b>A. List of isotopes for EEMEP simulations</b>	<b>40</b>

*Contents*

<b>B. Daily results of EEMEP run with one month release</b>	<b>50</b>
<b>C. Daily results of EEMEP run with six weeks release</b>	<b>54</b>

# 1. Introduction

This study is a part of the large EU project PREPARE with the title "Innovative integrative tools and platforms to be prepared for radiological emergencies and post-accident response in Europe". In the PREPARE project, the Norwegian Radiation Protection Authority (NRPA) is a full project partner, whereas the Norwegian Meteorological Institute (MET) is a sub-contractor of NRPA. The tasks for MET as a sub-contractor of NRPA involve both atmospheric part (60%) and marine part (40%). The tasks in the atmospheric part are related to developing and applications of the Eulerian dispersion model for the radioactive debris. The Assignment for MET includes the following:

- Develop parametrization of the source term in the Eulerian framework for radiological an nuclear releases.
- Establish an operational Eulerian dispersion model at MET.
- Make an interface between this model and the ARGOS system. The interface will use existing functionality inside ARGOS. This will allow results from the model to be viewed and analysed inside ARGOS.
- MET will apply methodology developed in WP4.4 to the Eulerian model. This way the model can be used to estimate the source term based on measurements from gamma dose rate monitors and measurements of particle concentration in the long range cases.

This is the first of the two reports in the project. The main topic of the first report is a preliminary version of the Eulerian EEMEP model and discussion of its initial applications in the ARGOS system. The EEMEP model is partly operational at MET at present and it is still under testing and development. The ARGOS system has been operational at NRPA for several years and it has been used as a tool for displaying and post-processing the results of the dispersion calculations for potential nuclear accidents and explosions.

Before the start of the PREPARE project, two dispersion models were available at MET: the Lagrangian model Severe Nuclear Accident Program (SNAP) as described in [3] and an experimental version of the Eulerian model which is currently under development. The SNAP model operates in regional scale with the spatial resolution approximately 12 km and the same computational domain (Fig. 1) as the Numerical Weather Prediction (NWP) model HIRLAM [21] which provides 66 hrs meteorological forecasts. The HIRLAM model is currently operational at MET, and its results serve as meteorological input for the SNAP model.

In the frame of a long term co-operation between NRPA and MET, the SNAP model has been used as a remote emergency tool in case of an nuclear accident [3]. The entire procedure is very fast and automatic. The system for remote application of SNAP from NRPA has been in operation for many years now and has proved to be robust. A similar system will be implemented for the Eulerian model operating at MET.

There is also an experimental version of the global SNAP model at MET. The domain of the global SNAP version is shown in Fig. 2

## 1. Introduction

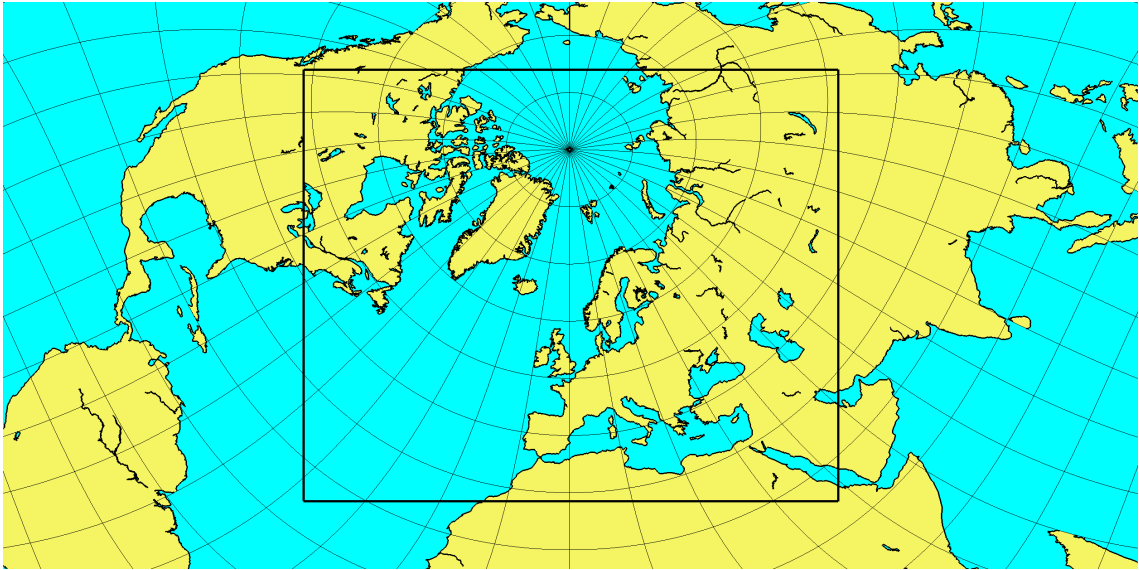


Figure 1: Computational domain of the operational SNAP model. It is also operational domain of the HIRLAM-12 NWP model at MET which is used as meteorological input provider for SNAP.

In general, atmospheric dispersion and transport of radioactivity can be modelled both in Lagrangian and Eulerian framework. Each approach has some advantages and disadvantages. The main advantages of the Lagrangian approach are:

- lack of the problems with artificial numerical diffusion when solving the advection equation,
- accurate parametrization of the point source geometry which is only described by the initial distribution of model particles and is independent on the fixed grid system,
- easy and natural parametrization of gravitational settling for large radioactive particles.

These advantages are especially useful for the simulations in regional scale of the size of 1000 km and therefore the Lagrangian SNAP model has been used as operational nuclear emergency model at MET since 1995 [12], [11], [13], [1]. There are also some disadvantages of the Lagrangian approach with the most of them being of computational nature:

- very large number of model particles and significant increase of computational time in case of long lasting accident. The execution time increase is more than linear with additional time of release, close to quadratic relation,
- very large number of model particles and significant increase of computational time (proportional to number of sources) in case of multiple sources,
- difficulties in calculating concentrations in the regions with a very low number of model particles,
- technical problems with parallel implementation of the code of Lagrangian model. The Lagrangian model performance depends on spatial resolution and a number of particles. Parallelization is technically difficult since the model particles need the information from the entire



model domain. A parallelization on  $N$  processors will require  $N$  times more memory.

Compared to Lagrangian models, the main advantages of the Eulerian approach are:

- lack of additional technical problems related to simulations with long and very long release of radionuclides, linear scaling in model-runtime, independent of release-time
- possibility of simulations of multiple sources active at the same time and no need for additional computer memory and additional computer time for such case,
- the execution time of the Eulerian model is proportional the forecast length and it is independent on the release period in the source term,
- possibility for easy parametrization of interactions between different molecules and aerosols, if necessary,
- easy way of parallel implementation of the code of Eulerian model on super-computer using domain decomposition and reducing both, real-time and memory per CPU usage.

The main disadvantages of the Eulerian approach can be listed as follows:

- problem with accurate parametrization of the source term geometry,
- some problems with artificial numerical diffusion especially close to the source,
- difficulties in parametrization of the gravitational settling process, especially for large particles

Many of the problems of lagrangian models can be efficiently solved in the Eulerian framework, especially in the large scales, like hemispheric or global. This is the main reason, why the Eulerian EEMEP model has been introduced into the MET emergency system. This model is used as pre-operational at present and will be used as fully operational in the future at MET. It is operating in the global scale covering the entire Earth. The global domain of the EEMEP system is shown in Fig. 2.

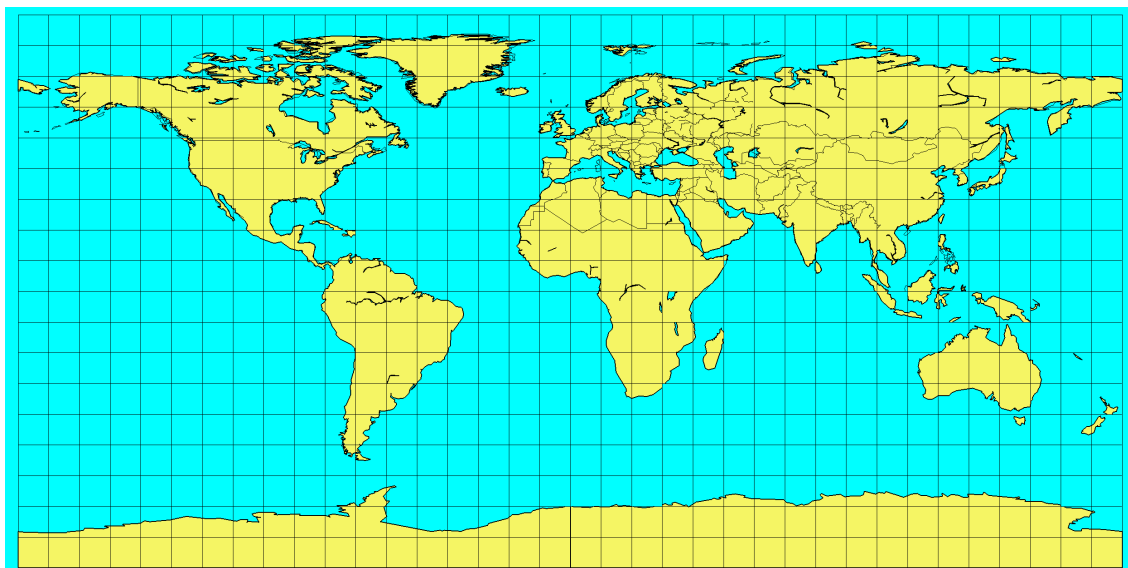


Figure 2: Computational domain of the global version of the EEMEP model and global version of the SNAP model at MET.

## 1. Introduction

In the second phase of the PREPARE project, the tools for better estimating the source term will be tested. These tools require a large number (several hundreds or more) of the model runs. A short execution time of the model is a great advantage in such applications of the dispersion calculations.

An important goal of the WP4 task of the PREPARE project is to improve dispersion modelling capabilities for long releases and possibly multiple sources. The Eulerian approach has some clear advantages over Lagrangian for such goals and is very promising, especially for the global scale. Therefore, in this study we focused on the development and applications of the Eulerian EEMEP model in the global scale. However, this issue is also very important in the regional scale with the potential accidents located within 1000 km from the receptor.

In principle, the EEMEP model can work efficiently in regional scale as well. However, in this scale a better spatial resolution is necessary. In the second phase of the project, we plan to test the EEMEP model in regional scale and compare its results with the results of Lagrangian SNAP model. The spatial resolution for this comparison will be much better than in the global scale - approximately 16 km.

In the future, the operational version of the EEMEP model developed at MET could be also used in other countries assuming that the necessary meteorological input is available. The EEMEP model is using global meteorological data from European Centre for Medium range Weather Forecast (ECMWF) at present, but it is also possible to use other sources of meteorological data as well. Therefore, the EEMEP model can be of interest to international nuclear emergency community, either for operational use or just for testing.

The EEMEP model is part of the EMEP-MSCW models which are made available as Open Source once a year and can in the future be downloaded from the following address:

[https://wiki.met.no/emep/page1/emepmscw\\_opensource](https://wiki.met.no/emep/page1/emepmscw_opensource).

## 2. Eulerian EEMEP Model

The Eulerian EEMEP model has been developed as a modification of the EMEP MSC-W model [16], [17], which has been used at MET since 1997 for modelling atmospheric transport of different pollutants over Europe. The EMEP MSC-W model has been developed in the framework of the European Monitoring and Assessment Program (EMEP) and used as operational at the Meteorological Synthesizing Centre - West (MSC-W) of EMEP located at MET.

### 2.1. Model equations

The basic equation of the Eulerian EEMEP model is the same as of the EMEP MSC-W model. It describes atmospheric transport and deposition of selected radionuclides and has the form of the continuity equation.

#### 2.1.1. Continuity equation

The mixing ratios are used in the continuity equation for all pollutants taken into account in the Eulerian model. The mixing ratio  $\chi$  is defined as the ratio of pollutant mass to mass of the air where this pollutant is located (kg of pollutant per kg of air). The continuity equation for the mixing ratio has the following form in the EEMEP model:

$$\begin{aligned} \frac{\partial}{\partial t}(\chi p^*) &= -m_x m_y \frac{\partial}{\partial x} \left( \frac{u}{m_y} \chi p^* \right) - m_x m_y \frac{\partial}{\partial y} \left( \frac{v}{m_y} \chi p^* \right) + \frac{\partial}{\partial \sigma} (\dot{\sigma} \chi p^*) + \\ &\quad \frac{\partial}{\partial \sigma} \left[ K_\sigma \frac{\partial}{\partial \sigma} (\chi p^*) \right] + \frac{p^*}{\rho} S \end{aligned} \quad (1)$$

The first three terms on the right hand side, in Eq. 1 represent three-dimensional advective transport. In the velocity field  $(u, v, \dot{\sigma})$ ,  $u$  and  $v$  are the horizontal velocity components and  $\dot{\sigma}$  is the vertical velocity in  $\sigma$ -coordinates ( $\dot{\sigma} = \frac{\partial \sigma}{\partial t}$ ). The  $m_x$  and  $m_y$  are the map factors in x- and y-direction, respectively. The fourth term on the right hand side, in Eq. 1 represents the vertical diffusion with  $K_\sigma$  being the vertical diffusion coefficient in  $\sigma$ -coordinates. Horizontal diffusion is not explicitly included in the EEMEP model. The variable  $S$  describes all sources and sink terms, e.g. emissions, radioactive decay, dry and wet deposition. The mass of pollutant in Eq. 1, used in the EMEP MSC-W model is substituted by the activity (in Bq) in the EEMEP model.

#### 2.1.2. Advection

The different terms in Eq. 1 are solved numerically applying different methods and algorithms. The advection part of the transport of Eq. 1 includes horizontal and vertical terms:

$$\left. \frac{\partial}{\partial t}(\chi p^*) \right|_{adv} = -m_x m_y \frac{\partial}{\partial x} \left( \frac{u}{m_y} \chi p^* \right) - m_x m_y \frac{\partial}{\partial y} \left( \frac{v}{m_y} \chi p^* \right) + \frac{\partial}{\partial \sigma} (\dot{\sigma} \chi p^*) \quad (2)$$

## 2. Eulerian EMEP Model

It is solved using the numerical algorithm developed by Bott [5], [6]. The fourth order version of this algorithm is applied to horizontal part of the advection term, whereas, a second order version, developed for irregular grid, is applied to vertical part of the advection term.

In the EMEP model, not only mass of each pollutant is advected using Botts algorithm, but mass of the air as well, assuming that the initial mixing ratio for air is equal to one. After each advection step the new mixing ratios are calculated by dividing the result by the new "air concentration":

$$\chi_x^{t+\Delta t} = \frac{(\chi_x P^*)^{t+\Delta t}}{(\chi_{air} P^*)^{t+\Delta t}} \quad (3)$$

where  $(\chi_x P^*)^{t+\Delta t}$  is the result obtained with the Bott algorithm for pollutant x after a time step  $\Delta t$ . This approach ensures mass conservation of pollutant during the advection which otherwise can be disturbed by the divergence present in the velocity field.

### 2.1.3. Vertical diffusion

The diffusion part of the transport Eq. 1 includes only vertical term:

$$\left. \frac{\partial}{\partial t} (\chi P^*) \right|_{diffusion} = \frac{\partial}{\partial \sigma} \left[ K_\sigma \frac{\partial}{\partial \sigma} (\chi P^*) \right] \quad (4)$$

It is assumed in the EMEP model that numerical diffusion in the solution of the advection part of Eq. 1 is of the same magnitude as the physical horizontal diffusion. Therefore, it is neglected in the Eq. 1 and only vertical diffusion is included. An implicit algorithm is used for the numerical solution of Eq. 4.

### 2.1.4. Convection

Convection and especially deep convection is a very important process for dynamics of air pollution because it is responsible for relatively fast displacement of pollutants in vertical direction. This transport is much faster than transport through large scale advection. Convection is rather difficult to parametrize in air pollution models [18], but it cannot be neglected in all scales and for simulations in the global-scale good parametrization of convection is essential.

The convective mass flux scheme applied in the EMEP model is the same as in EMEP MSC-W model and is based on Tiedtke [20]. This scheme is the same as used in the Oslo CTM2 model [4]. The meteorological input for the calculations is a convective up-draft mass flux, provided at every level in each model column. The so called elevator principle is applied for calculating the convective transport of pollutant mass. The numerical implementation of the convective routine in the EMEP MSC-W model is explained in Simpson et al. [16], [17].

### 2.1.5. Source term for nuclear accident

The source geometry is time dependent in the EMEP model and can be specified differently for each time segment of the release during the nuclear accident. The source term can be also

specified separately for each substance which is released into the atmosphere. The release rate is defined separately for each component released and can vary in time. The source term parametrization in EEMEP is very similar to parametrisation in SNAP [3], second operational model at MET. The main differences are related to different geometries of the source terms in both models.

The radionuclides released during the nuclear accident and simulated by EEMEP can be in the form of noble gases, gases and particles. There is a list of 382 isotopes important for NRPA which are included in ARGOS system and can be simulated by the EEMEP model. For each isotope on the list, the name of it, type (noble gas, aerosol and Iodine) and decay rate are specified. The list is presented in Appendix A.

Most of radionuclides included in the EEMEP model are in the form of aerosol with particle size of the order of  $1\ \mu\text{m}$ . Therefore, gravitational settling velocity can be neglected for those components allowing shorter computational time. Aerosols are subject to dry and wet deposition during the transport, with wet deposition being more effective than dry deposition in removing aerosols from the air. Gases are mostly represented by different form of Iodine. The noble gases are not affected by dry and wet deposition and because of that, they can stay in the atmosphere for a long time. The following noble gases can be included in the EEMEP model: Ar, Kr, Rn and Xe.

The vertical geometry of the source for nuclear accident is usually specified by the vertical range given in meters above the ground. In the model calculations, this vertical range is transformed into corresponding model layers, in most cases below the mixing height. Horizontal size of the source geometry is limited by the size of the horizontal model grid square, which is  $1\ \text{deg} \times 1\ \text{deg}$  for the global version of the EEMEP model. Such approach leads to significant underestimation of the initial concentrations close to the accident location in the current preliminary version of the EEMEP model. This problem will be eliminated in the second phase of the project when a better parametrization of the source term for nuclear accident in the frame of Eulerian approach will be developed.

### 2.1.6. Source term for nuclear detonation

The source term for nuclear explosions in the EEMEP model is very similar to the source term implemented in the Lagrangian SNAP model, also operational at MET. A major difference is caused by the poor spatial resolution of the global grid of the EEMEP model. In the Eulerian model the radioactive cloud after explosion is assumed to be uniformly distributed over the square of the size  $1\ \text{deg} \times 1\ \text{deg}$ , whereas in the Lagrangian model, the radioactive particles are distributed in the cylinder with relatively small radius (maximum 8.5 km). So, in the EEMEP model, the initial distribution of radioactive particles has a shape of the box with a vertical range dependent on the explosive yield.

The activity and geometry of the source term for nuclear detonation is mainly determined by the explosive yield [10], [14], [2]. Eight classes of explosive yields are taken into account in the EEMEP model: 1 kt, 3 kt, 10 kt, 30 kt, 100 kt, 300 kt, 1000 kt and 3000 kt. Parameters for the initial box and activities, depending on eight explosive yield classes, are given in Table 1.

As in case of nuclear accident, vertical ranges of the boxes specified in Table 1, for nuclear explosion, have to be transformed into the model layers before the model runs. These model

## 2. Eulerian EMEP Model

Table 1: Parameters for the box, for the radioactive cloud shortly after the explosion and activities for explosive yield classes. The base of the box has the size 1 deg × 1deg.

Explosive yield (kt)	Base of the box (km)	Top of the box	Activity (Bq)
1	0.50	1.50	$2 \times 10^{19}$
3	1.40	3.10	$6 \times 10^{19}$
10	2.25	4.75	$2 \times 10^{20}$
30	4.10	8.40	$6 \times 10^{20}$
100	5.95	12.05	$2 \times 10^{21}$
300	8.00	18.50	$6 \times 10^{21}$
1000	10.00	25.00	$2 \times 10^{22}$
3000	12.00	32.00	$6 \times 10^{22}$

layers can be located very high above the ground and inaccuracy introduced by the transformation can be significant. To solve this problem a special parametrization of the source term for nuclear explosion will be developed in the second phase of the project.

### 2.1.7. Dry deposition

Dry and wet depositions are the most important processes responsible for removing pollutants from the air. Dry deposition is different for different pollutants and is determined not only by meteorological conditions, but also by the type and state of the surface on which dry deposition occurs. There are some similarities in dry deposition parametrization for three kinds of pollutants included in the EMEP model: gases, aerosols and particles. Therefore, parametrization of dry deposition will be described separately for these three kinds of pollutants.

**Dry deposition of gases** The resistance analogy is used in parametrization of dry deposition for gases in the EMEP model. The dry deposition flux  $F_g^i$  of gas  $i$  to the ground surface is calculated using the deposition velocity  $V_g^i(z)$  and following equation [16], [17]:

$$F_g^i(z) = -V_g^i(z) \cdot \chi^i(z) \quad (5)$$

This equation is valid in the constant flux layer. The concentration and deposition velocity in the model are calculated in the centre of the lowest grid cell, typically 45 m above the surface. It is assumed to be within the constant flux layer. Deposition velocity is calculated using a resistance approach:

$$V_g^i(z) = \frac{1}{R_a(z) + R_b^i + R_c^i} \quad (6)$$

where  $R_a$  is the aerodynamic resistance between the height  $z$  and the top of the vegetation canopy (formally,  $d + z_0$ , where  $d$  is the displacement height and  $z_0$  the roughness length),  $R_b^i$  is the quasi-laminar layer resistance to gas  $i$ , and  $R_c^i$  is the surface (canopy) resistance. For the

grids over sea, meteorological parameters from NWP models are used to calculate resistances in Eq. 6. For the grid with mixture of different land classes, the so-called mosaic approach is used. The grid average deposition rate is given by:

$$\tilde{V}_g^i(z) = \sum_{k=1}^N f_k \cdot V_{g,k}^i(z) \quad (7)$$

where  $\tilde{V}_g^i(z)$  is the grid-square average deposition velocity,  $f_k$  is the fraction of land-cover type  $k$  in the grid-square, and  $V_{g,k}^i$  is the deposition velocity for this land-cover type.

**Dry deposition of aerosols and particles** Compared to gases a relatively simple scheme is implemented in the EEMEP model for calculating dry deposition velocity for aerosols. First, the surface deposition velocity  $V_{ds}$  is estimated by the equation:

$$V_{ds} = \begin{cases} a_1 F_N & L \geq 0 \\ a_1 F_N \left[ 1 + \left( \frac{-a_2}{L} \right)^{2/3} \right] & L < 0 \end{cases} \quad (8)$$

where  $F_N = 3$  for nitrates and 1 for all other compounds in the EMEP MSC-W model and  $F_N = 1$  for all aerosols in the EEMEP model. The application of Eq. 8 is restricted to  $1/L > -0.04 \text{ m}^{-1}$ . For all land cover categories except forests, the value  $a_1 = 0.002$  is used [23] and  $a_2 = 300 \text{ m}$  as a simplified stability correction suggested by Gallagher et al. [7]. For forests,  $a_1$  is a function of Surface Area Index SAI:

$$a_1 = 0.008 \frac{SAI}{10} \quad (9)$$

Eq. 9 is used with the restriction  $a_1 \geq 0.002$  and  $a_2$  set again to 300 m. In addition, a minimum value for the surface dry deposition velocity  $V_{ds} \geq 0.002 \cdot U_*$  is enforced in Eq. 8. Following Venkatram and Pleim [22], the resistance analogy is not appropriate for particles. Therefore, the following mass-conservative equation is used in the EMEP MSC-W and EEMEP models:

$$V_d(z) = \frac{v_s}{1 - a^{-r(z)v_s}} \quad (10)$$

where  $v_s$  is settling velocity,  $V_d(z)$  is the deposition velocity at height  $z$ , and  $r(z)$  is the sum of the aerodynamic resistance and inverse  $V_{ds}$ .

### 2.1.8. Wet deposition

Wet deposition processes in the EEMEP model take into account both in-cloud and below-cloud scavenging. Parametrization of in-cloud scavenging is the same for gases and particles, whereas parametrization of below-cloud scavenging is different.

**In-cloud scavenging** The in-cloud scavenging of soluble component  $\chi$  (gas or particle) is described by the following equation:

## 2. Eulerian EEMEP Model

$$S_{in} = -\chi \frac{W_{in}P}{h_s\rho_w} \quad (11)$$

where  $W_{in}$  is in-cloud scavenging specified separately for each component [16], [17] is the precipitation rate,  $h_s$  is the characteristic scavenging depth, assumed to be 1000 m and  $\rho_w$  is the water density ( $1000 \text{ kg m}^{-3}$ ). The possible effect that dissolved material can be released if clouds or rain water evaporates is not taken into account in the EEMEP model.

**Below-cloud scavenging** Parametrization of below-cloud scavenging is different for gases and particles in the EEMEP model. The sub-cloud scavenging of gases is calculated according to the following equation:

$$S_{gas}^{sub} = -\chi \frac{W_{sub}P}{h_s\rho_w} \quad (12)$$

where  $W_{sub}$  is the sub-cloud scavenging ratio specified for each component in gas state. For particles, wet deposition rates are calculated based on Scott [15]:

$$S_{aer}^{sub} = -\chi \frac{AP}{V_{dr}} \tilde{E} \quad (13)$$

where  $V_{dr}$  is the the raindrop fall speed ( $V_{dr} = 5 \text{ m s}^{-1}$ ),  $A = 5.2 \text{ m}^3 \text{ kg}^{-1} \text{ s}^{-1}$  is the empirical coefficient (a Marshall-Palmer size distribution is assumed for rain drops), and  $\tilde{E}$  is the size-dependent collection efficiency of aerosols by the raindrops. The collection efficiency is size dependent, with a minimum for fine particles (see Laakso et al. [9] and Henzing et al.[8]).

### 2.1.9. Radioactive decay

All isotopes included in the EEMEP model are subject to radioactive decay. For radionuclides listed in Appendix A which are used in the model runs, radioactive decay is described by the decay constant. The relation between half-life time  $T_{1/2}$  and decay constant  $\lambda$  is the following:

$$T_{1/2} = \frac{\ln 2}{\lambda} = \frac{0.693}{\lambda} \quad (14)$$

The activity of any isotope remaining in the air after time  $t$  is calculated according to the following equation:

$$A(t) = A_0 e^{-\lambda t} \quad (15)$$

where  $A(t)$  is the activity at time  $T$  and  $A_0$  is the initial activity of the considered isotope. The calculations are performed at every time step  $\Delta t$ , so:

$$A(t + \Delta t) = A(t) e^{-\lambda \Delta t} \quad (16)$$

The radioactive decay is also affecting a part of each isotope already deposited to the ground, so the same approach is applied to matrices of wet and dry deposition for each isotope at each model time step:



$$\begin{aligned} D_{dry}(i, j, t + \Delta t) &= D_{dry}(i, j, t)e^{-\lambda t} \\ D_{wet}(i, j, t + \Delta t) &= D_{wet}(i, j, t)e^{-\lambda t} \end{aligned} \quad (17)$$

where  $D_{dry}(i, j, t)$  and  $D_{wet}(i, j, t)$  are matrices of dry and wet deposition respectively.

## 2.2. Operational applications of EEMEP model

The main objective of operational application of the EEMEP model is the help for meteorologists on duty in case of nuclear accident or explosion. The EEMEP model is run automatically every day for selected locations of potential accidents and explosions. In the situation with a real accident, meteorologist on duty can examine the results of existing model runs very fast to come up with the first evaluation of the emergency level.

In the future, the EEMEP model will be also implemented for remote on-line applications from NRPA for simulating nuclear accidents and explosions in global scale.

### 2.2.1. Operational set-up

In the present operational application at MET the EEMEP model is run two times each day to simulate dispersion of radioactivity from potential nuclear accidents and potential detonations. The model is updated two times daily, at 09:10 and 21:10 local winter time, based on analysis at 00 and 12 UTC respectively. The 00-UTC run is forecasting four days ahead, and the 12-UTC run is forecasting three days ahead. As soon as, the results of EEMEP model simulations are ready, they can be easily displayed in the DIANA graphic system operational at MET.

### 2.2.2. Nuclear accidents

Atmospheric transport of five radionuclides is simulated by the EEMEP model: Cs-137, I-131, Kr-85, Sr-90 and Xe-133. For this radionuclides, hourly instantaneous concentrations and time integrated concentrations from the start of the forecast are calculated.

The sources of potential nuclear accidents are in fixed locations in the nuclear power plants which could effect Norway. The list of these NPPs is shown in Table 2. The choice of the operational sources was suggested by NRPA.

### 2.2.3. Nuclear explosions

The source term for nuclear explosions in the EEMEP model is very similar to the source term implemented in the Lagrangian SNAP model, also operational at MET. A major difference is caused by the poor spatial resolution of the global grid of the EEMEP model. Whereas in the Lagrangian model, the release in case of nuclear accident has a cylinder shape of the relatively small radius (maximum 5 km), the horizontal resolution of the EEMEP model is approximately 300 km.

Two locations for potential nuclear explosions have been selected for operational EEMEP runs: Teheran and a location in Nord Korea. As in case of nuclear accident, the locations of potential nuclear detonations were also suggested by NRPA.

## 2. Eulerian EEMEP Model

Table 2: NPPs selected as sources of potential nuclear accidents in the operational runs of EEMEP model. Latitude and longitude in decimals.

Name of NPP	Country	Long., Lat.
Brokdorf	Germany	9.35, 53.85
Forsmark	Sweden	18.18, 60.40
Kola	Russia	32.47, 67.47
Leningrad	Russia	29.04, 59.84
Loviisa	Finland	26.39, 60.37
Olkiluoto	Finland	21.54, 61.22
Oskarshamn	Sweden	16.67, 57.42
Ringhals	Sweden	12.10, 57.25
Sellafield	United Kingdom	-3.50, 54.42
Torness	United Kingdom	-2.41, 55.97

### 2.2.4. On demand simulations

It should be mentioned here, that in case of a real emergency, meteorologists can perform additional runs of the EEMEP model with up to three additional nuclear explosions or one nuclear accident. The place and the start-time of the accident have to be specified, as well as the explosive yield of the nuclear bomb. In case of nuclear accidents, the amount of emissions is usually unknown in the beginning phase, and default values will be used.

## 2.3. Results of the operational EEMEP model

The results of the operational EEMEP model runs are available to meteorologist on duty every day. They can be displayed using DIANA system at MET. Some examples of such results for nuclear accidents and nuclear explosions are presented here. First, the results for nuclear accidents are shown.

### 2.3.1. Results for nuclear accidents

For simulation of nuclear accidents, the EEMEP was used to forecast 96 hours of atmospheric transport of four radionuclides: Sr-90, I-131, Xe-133 and Cs-137. The start of hypothetical accidents was assumed on 28 January 2014 at 00 UTC. In Figs 3 - 12 the results of the model simulations for 96 hours forecast are presented, for the releases in all NPPs listed in Table 2. The examples are presented here in the entire global model domain, just for the illustration of the global perspective. The resolution of the global maps presented here is rather poor and the details not well seen. However, in the DIANA graphic system, available to meteorologist on duty, much better resolution is possible, as well as arbitrary zooming of the results. It is also possible to see three-dimensional model results in this system.

### 2.3. Results of the operational EEMEP model

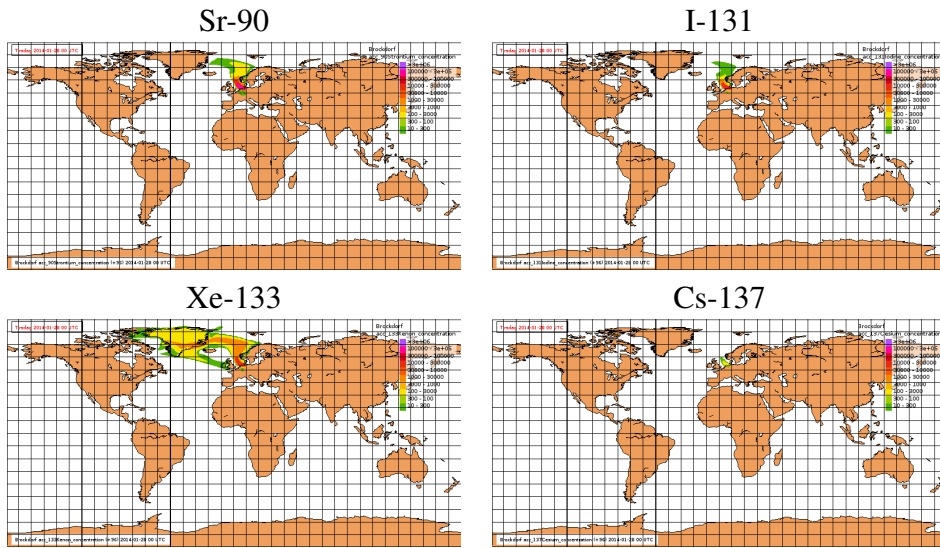


Figure 3: Operational forecast from the EEMEP model for 96 hours. Time integrated concentrations of Sr-90, I-131, Xe-133 and Cs-137 (Bq h m<sup>-3</sup>) for potential accident at Brokdorf NPP.

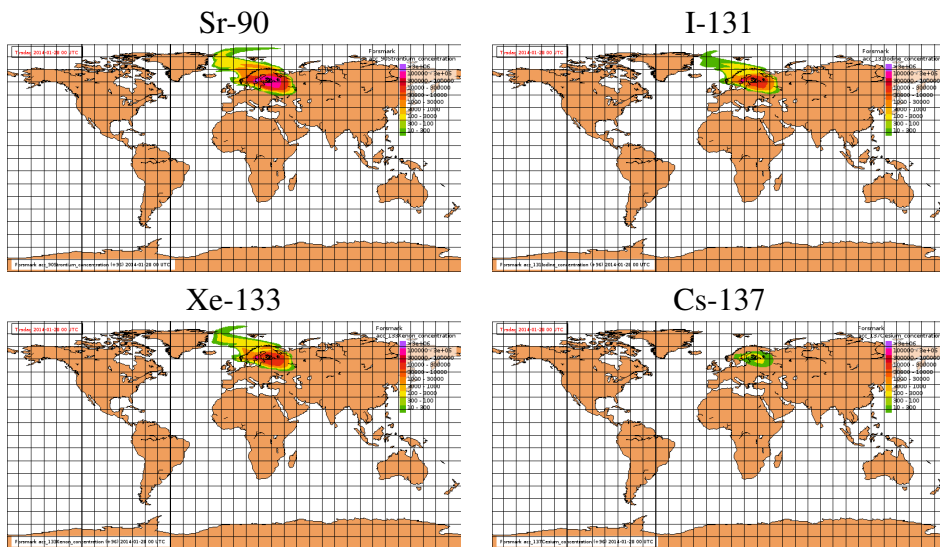


Figure 4: Operational forecast from the EEMEP model for 96 hours. Time integrated concentrations of Sr-90, I-131, Xe-133 and Cs-137 (Bq h m<sup>-3</sup>) for potential accident at Forsmark NPP.

## 2. Eulerian EMEP Model

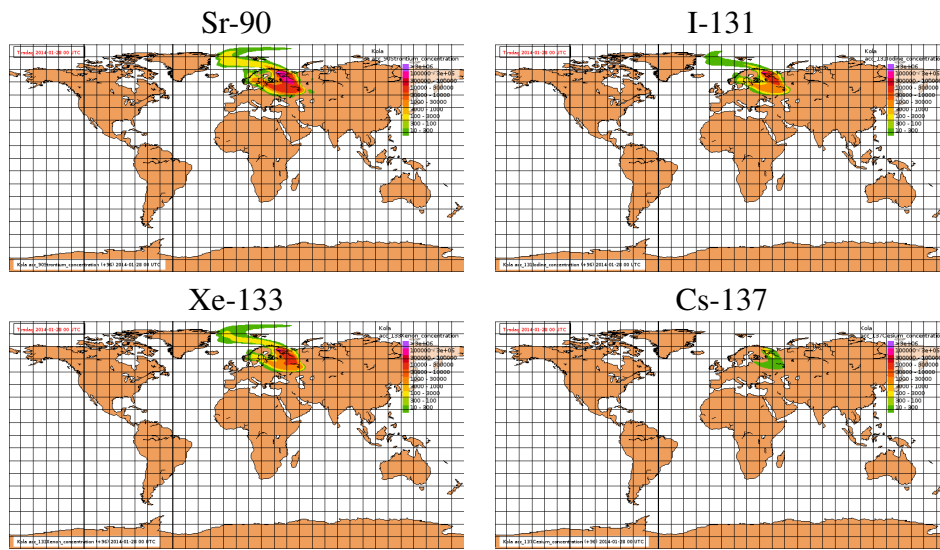


Figure 5: Operational forecast from the EMEP model for 96 hours. Time integrated concentrations of Sr-90, I-131, Xe-133 and Cs-137 (Bq m<sup>-3</sup>) for potential accident at Kola NPP.

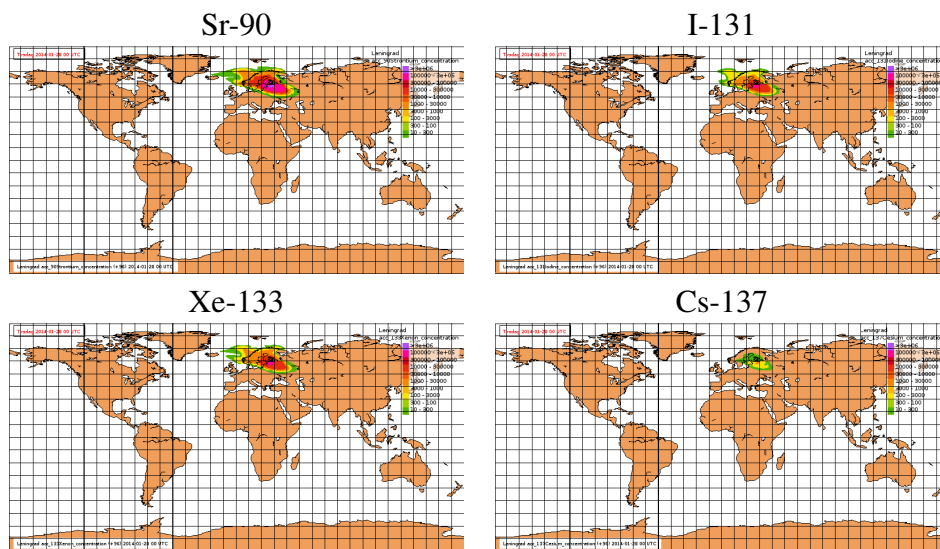


Figure 6: Operational forecast from the EMEP model for 96 hours. Time integrated concentrations of Sr-90, I-131, Xe-133 and Cs-137 (Bq h m<sup>-3</sup>) for potential accident at Leningrad NPP.

### 2.3. Results of the operational EEMEP model

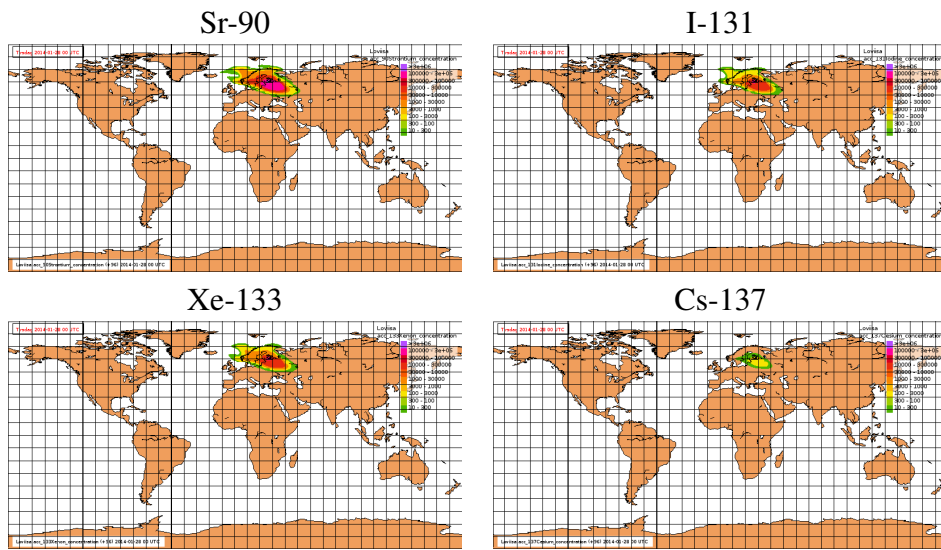


Figure 7: Operational forecast from the EEMEP model for 96 hours. Time integrated concentrations of Sr-90, I-131, Xe-133 and Cs-137 ( $\text{Bq h m}^{-3}$ ) for potential accident at Loviisa NPP.

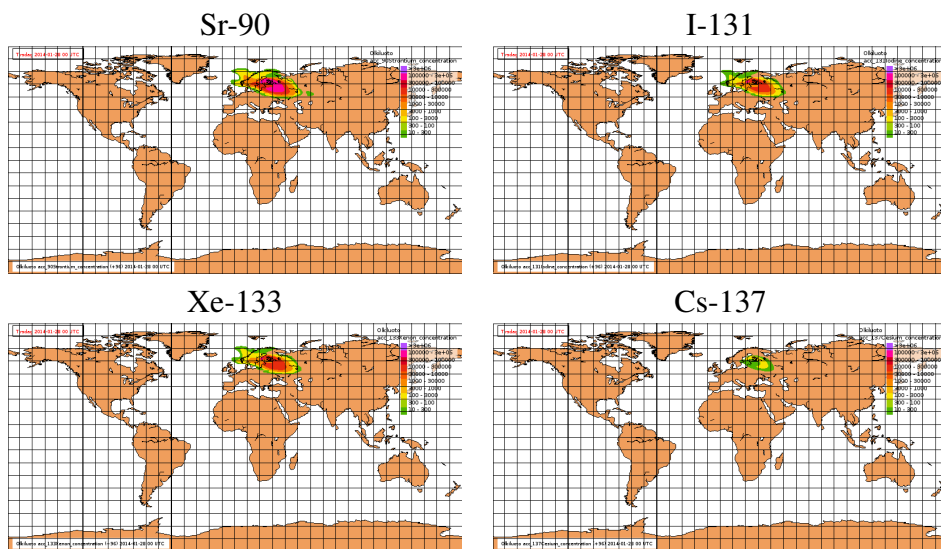


Figure 8: Operational forecast from the EEMEP model for 96 hours. Time integrated concentrations of Sr-90, I-131, Xe-133 and Cs-137 ( $\text{Bq h m}^{-3}$ ) for potential accident at Olkiluoto NPP.

## 2. Eulerian EMEP Model

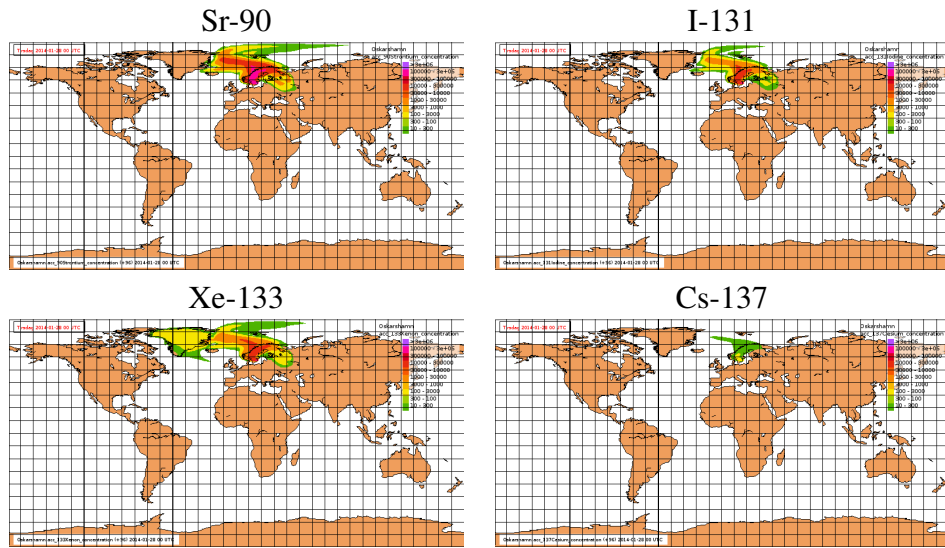


Figure 9: Operational forecast from the EEMEP model for 96 hours. Time integrated concentrations of Sr-90, I-131, Xe-133 and Cs-137 ( $\text{Bq h m}^{-3}$ ) for potential accident at Oskarshamn NPP.

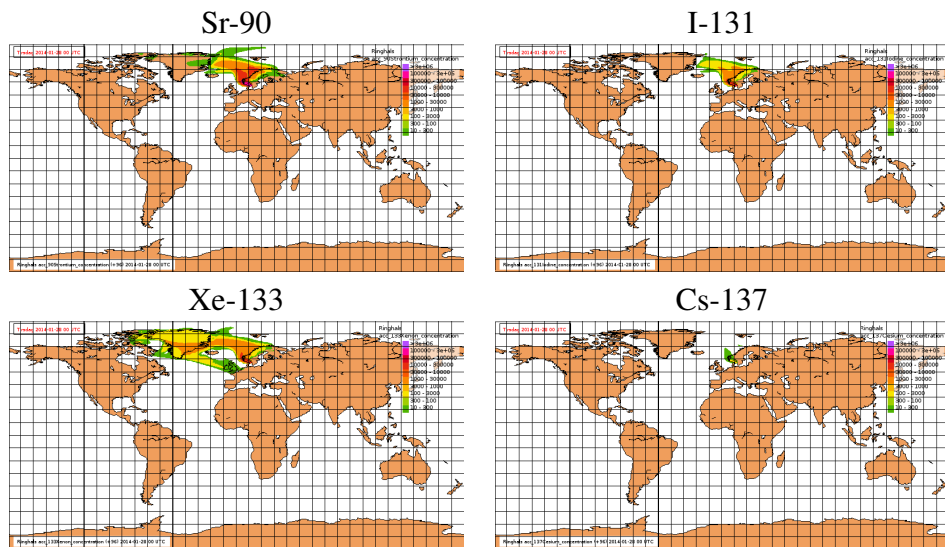


Figure 10: Operational forecast from the EEMEP model for 96 hours. Time integrated concentrations of Sr-90, I-131, Xe-133 and Cs-137 ( $\text{Bq m}^{-3}$ ) for potential accident at Ringhals NPP.

### 2.3. Results of the operational EEMEP model

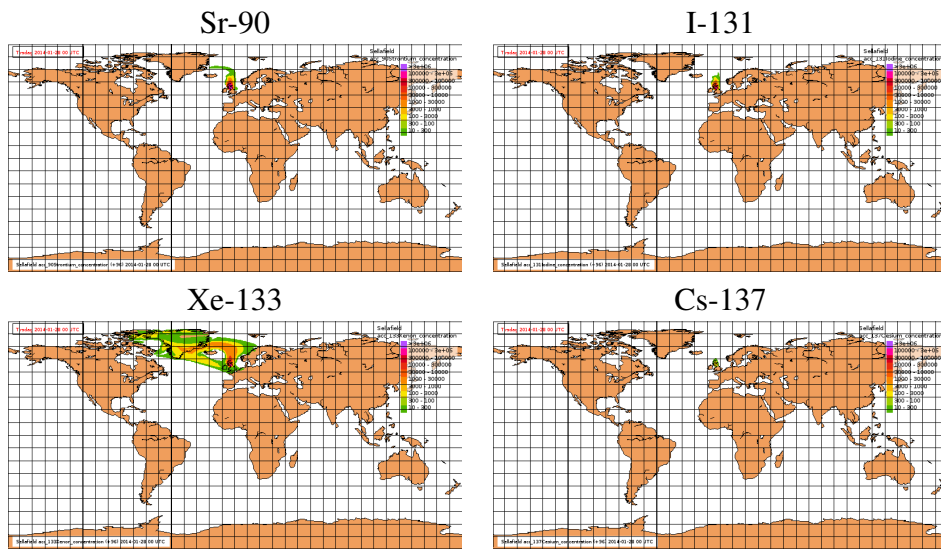


Figure 11: Operational forecast from the EEMEP model for 96 hours. Time integrated concentrations of Sr-90, I-131, Xe-133 and Cs-137 ( $\text{Bq h m}^{-3}$ ) for potential accident at Sellafield NPP.

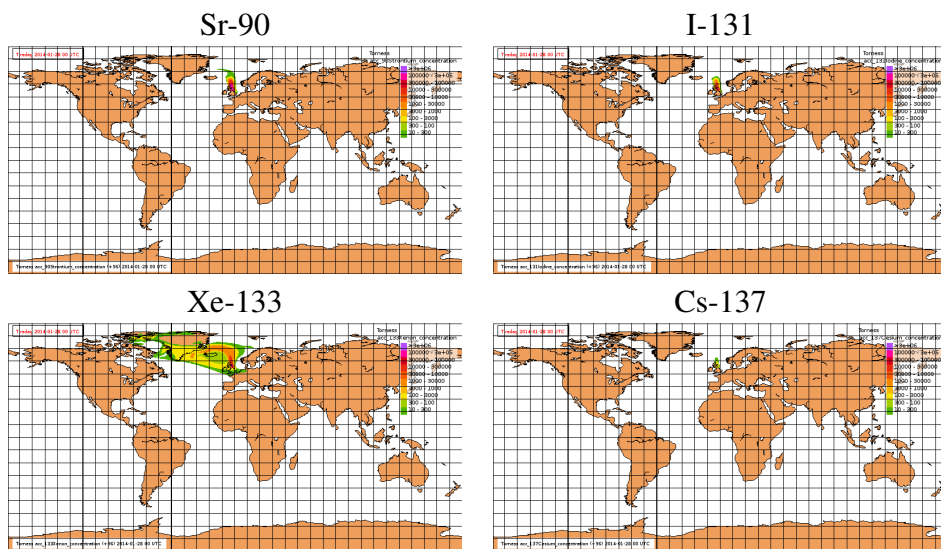


Figure 12: Operational forecast from the EEMEP model for 96 hours. Time integrated concentrations of Sr-90, I-131, Xe-133 and Cs-137 ( $\text{Bq h m}^{-3}$ ) for potential accident at Torness NPP.

## 2. Eulerian EEMEP Model

### 2.3.2. Results for nuclear explosions

For simulation of nuclear explosions, the EEMEP model was used to forecast 96 hours of atmospheric transport of radioactive particles. The start of hypothetical accidents was also assumed on 28 January 2014 at 00 UTC. Both, simulation of nuclear accidents and nuclear explosions were performed in the same run of the EEMEP model. In Fig. 13 the results of the model simulations for 96 hours forecast are presented, for two explosion locations listed in Table 2. As in case of nuclear accidents, the examples are presented in the entire global model domain, just for illustration of the global perspective.

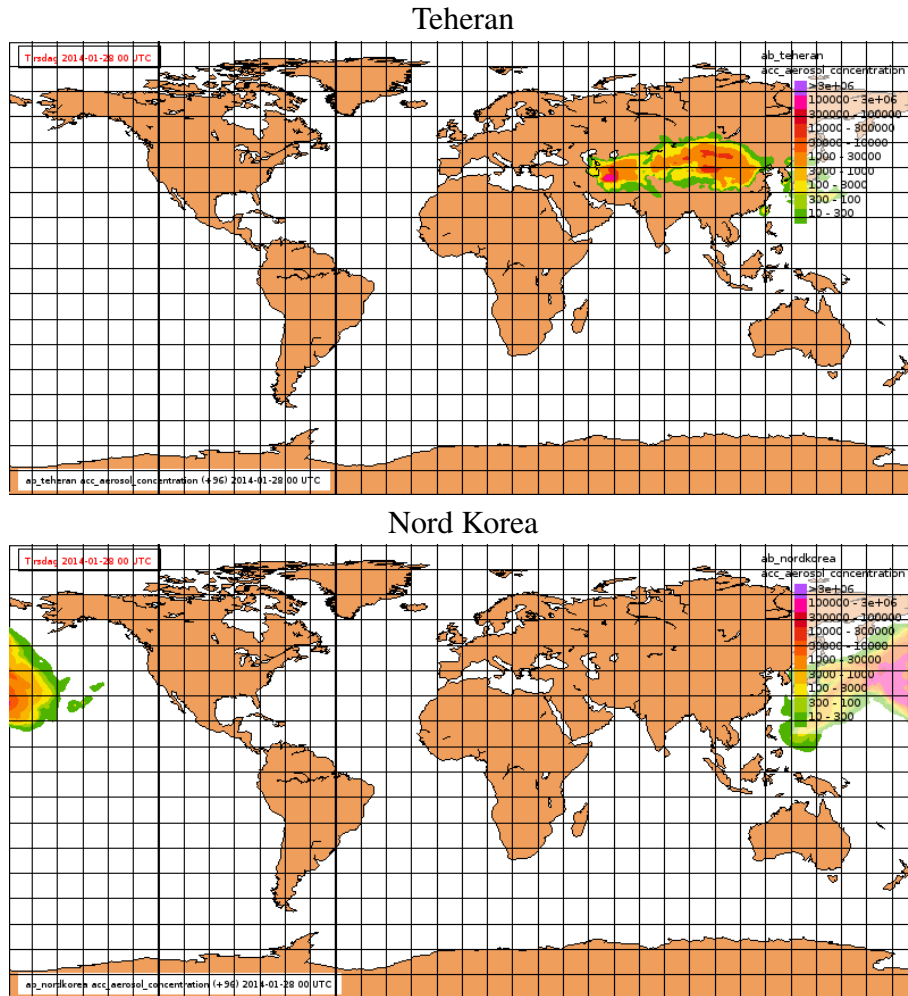


Figure 13: Operational forecast from the EEMEP model for 96 hours. Time integrated concentrations of radioactive aerosol from nuclear explosion in Teheran (above) and in Nord Korea (below). Units:  $\text{Bq h m}^{-3}$ .



### **3. Model simulation for long term release**

One of the advantages of the EULERIAN model is the efficient simulation of the accident with long or very long period of release. To test this model ability, the EEMEP model was run for the source term with one month with constant release and for three months period with variable release of Cs-137 and Xe-131 lasting six weeks. As a test case for the Eulerian EEMEP model the Fukushima location and accident period was chosen. The start of the model simulations was the same as the start of the Fukushima accident - 11 March 2011.

#### **3.1. Source term for long release**

Two different source terms were used for testing the EEMEP model with long term release, first one with constant release rate and the second with the release rate variable in time. Both tests are difficult for Lagrangian models because of extremely large number of model particles which have to be released for such source terms. We expected less problems with running the Eulerian model for the selected source terms.

##### **3.1.1. Source term with constant emissions**

In the first sources term, constant emissions for Xe-133 and Cs-137 were specified for the period 11 march 2011 - 10 April 2011. The constant release rates were relatively high:  $1.0 \times 10^{13} \text{ Bq s}^{-1}$  and  $1.0 \times 10^{10} \text{ Bq s}^{-1}$ , for Xe-133 and Cs-137, respectively. The length of release was 744 hours from the accident start, which means total release of  $2.68 \times 10^{19} \text{ Bq}$  and  $2.68 \times 10^{17} \text{ Bq}$ , for Xe-133 and Cs-37, respectively. The vertical range of the release was from 0 to 1000 m above the ground for both isotopes. This vertical range was automatically transformed into corresponding model layers during the model run. The EEMEP model with the constant release source term was run for the same period as the release length - one month.

##### **3.1.2. Source term with variable emissions**

In the second source term, the variable in time emissions of Xe-131 and Cs-137 are specified for the model runs. In this case, we have used more realistic releases of Xe-133 and Cs-137 during the Fukushima accident as estimated in Stohl [19]. These emissions are shown in Fig. 14. The EEMEP model with the variable emissions was run for three months period, starting from the beginning of Fukushima accident.

#### **3.2. Model results for long release simulations**

The results of two EEMEP model runs with long releases of radionuclides are shown as different maps. The results of the first run, with constant emissions for the same period as release - one month, are shown as maps of time integrated concentrations. The results of the second run, with more realistic emissions as presented in [19], are shown as maps of instantaneous concentrations.

### 3. Model simulation for long term release

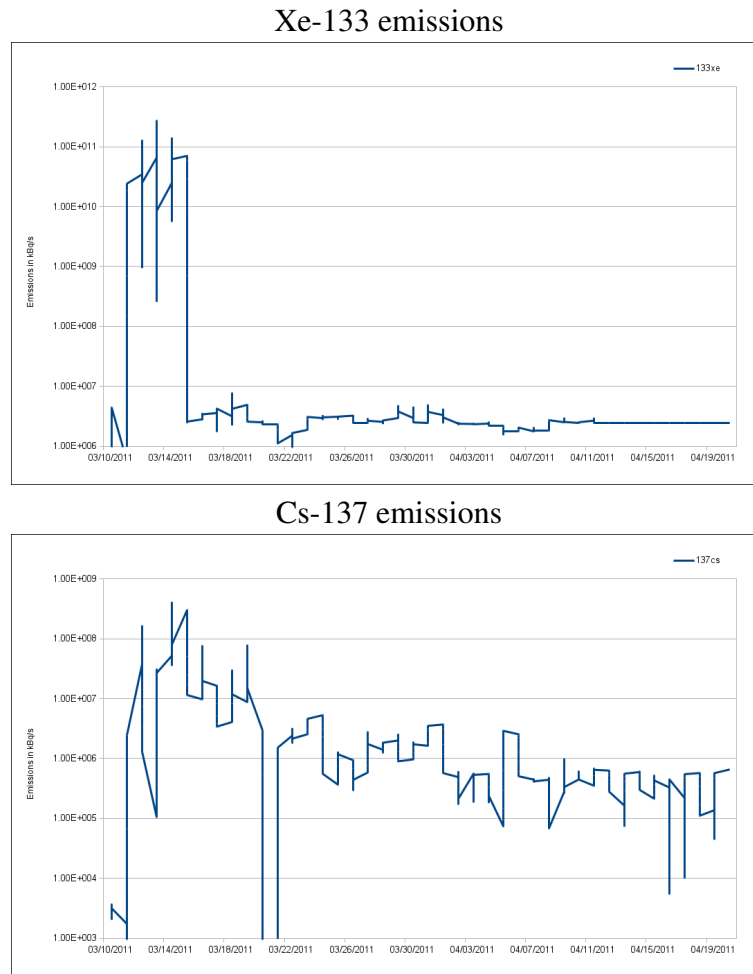


Figure 14: Emissions of Xe-133 and Cs-137 for long term model run with three months simulation.

The argument for difference in the outputs is the following. For the continues release, time integrated concentrations are relatively large over the entire model domain and they look good on the map. For variable release, time integrated concentrations are very high at the source, but very small and hardly visible far away from the source. The dynamic is too large to show them correctly. So, we decided to use different maps for two releases simulated.

#### 3.2.1. Results for the release with constant emissions

Some examples of the model results for the release with constant emissions are shown in Fig. 15, as maps of time integrated concentrations, after 10 days from the release start and after 31 days from the release start. The maps are shown for two isotopes: Xe-133 noble gas and Cs-137 - aerosol. As expected, there is much more Xe-133 remaining in the air than Cs-137 after any period of transport, because Xe-133 is not effected by the deposition processes.

### 3.2. Model results for long release simulations

A complete set of maps of time integrated concentrations for the simulation with constant emissions is given in Appendix B, for Xe-133 and Cs-137, for each day of the simulation.

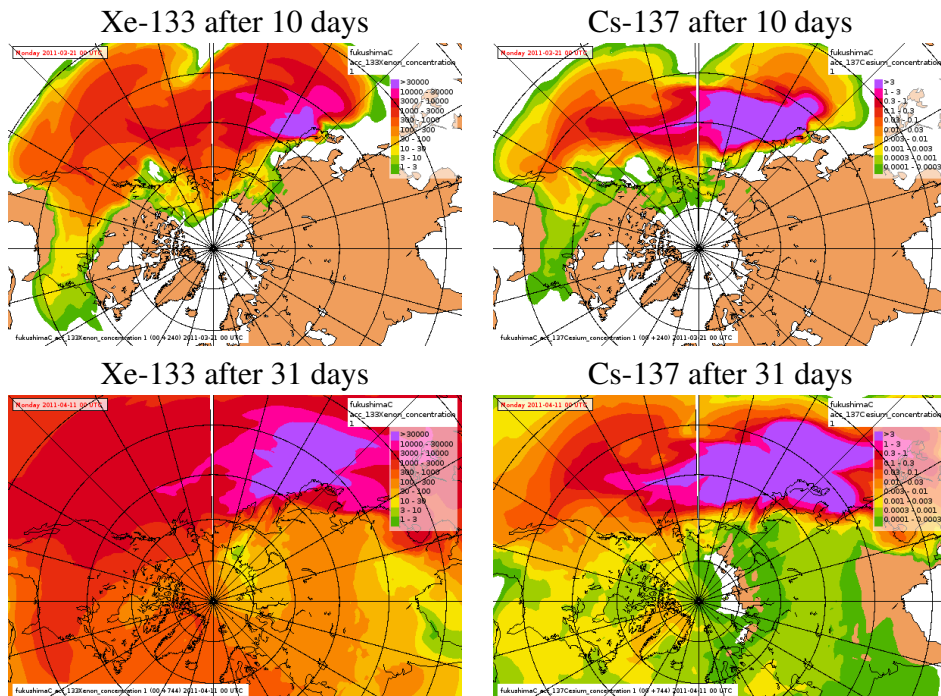


Figure 15: Time integrated concentration after 10 days from the start of the constant release (above) and after 31 days of the simulation (below). The results for Xe-133 on the left and for Cs-137 on the right. Units Bq h m<sup>-3</sup>.

#### 3.2.2. Results for the release with variable emissions

The examples of the model results for the release with more realistic variable emissions are shown in Fig. 16, as maps of instantaneous concentrations, after 20 days from the release start and after 50 days from the release start. The maps are shown for two isotopes: Xe-133 noble gas and Cs-137 - aerosol. Also in this simulation, there is much more Xe-133 remaining in the air than Cs-137, for any period of transport. The release stops after six weeks and practically the concentration of Cs-137 is zero everywhere after 60 days of the simulation. The concentration of Xe-133 is still present on the maps after 88 days. A complete set of maps of time instantaneous concentrations for the simulation with variable emissions is given in Appendix C, for Xe-133 and Cs-137, for each day of the simulation.

### 3. Model simulation for long term release

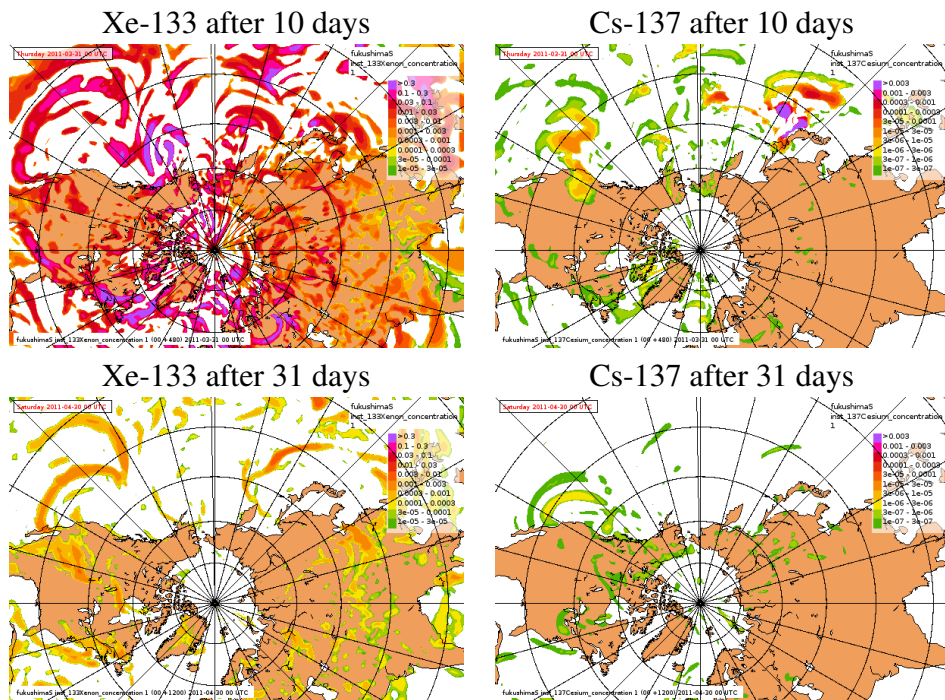


Figure 16: Instantaneous concentration after 20 days from the start of release with variable emissions (above) and after 50 days from the release start (below). The results for Xe-133 on the left and for Cs-137 on the right. Units Bq m<sup>-3</sup>.

## 4. Preliminary comparison of model results with measurements

For comparison of model results with the measurements, we have used the Fukushima accident and "A posteriori" emissions from Stohl [19]. This comparison has not been an easy task and it was not possible in full extent, because we haven't been able to access sufficiently good time-series of measurement data. As Stohl [19] points out, virtually no datasets related to Fukushima accident are publicly available, however, the results of measurements in selected sites can be found in his paper. Therefore, we have used the measurement data published in Stohl et al. [19] in our comparison. These data include concentrations of Cs-137 at three stations: Tokai-mura, Oahu (Hawaii) and Stockholm. The locations of these stations are shown in Fig. 17.

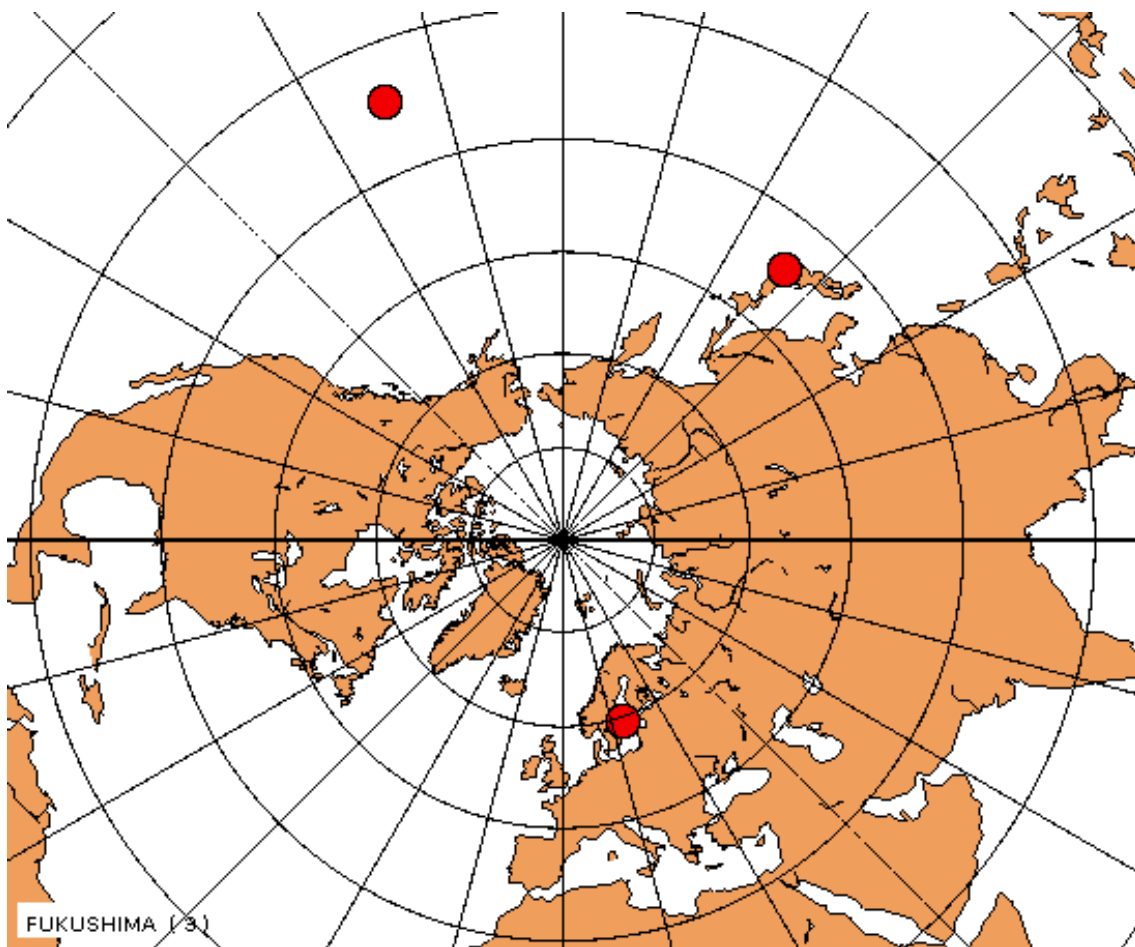


Figure 17: Preliminary comparison with measurements. The locations of three measurement stations: Tokai-mura, Oahu (Hawaii) and Stockholm, used for comparison of Cs-137 concentrations with EEMEP model results.

#### 4. Preliminary comparison of model results with measurements

Time series of observed Cs-137 concentrations at Tokai-mura, Oahu and Stockholm stations are shown in Fig. 18 as black lines. In addition, the model results obtained by Stohl with the FLEXPART model are shown in this figure and are marked with different colours. The results of the EEMEP model run for Fukushima accident, at the same three stations, in the form of time series of the surface concentrations are shown in Fig. 19.

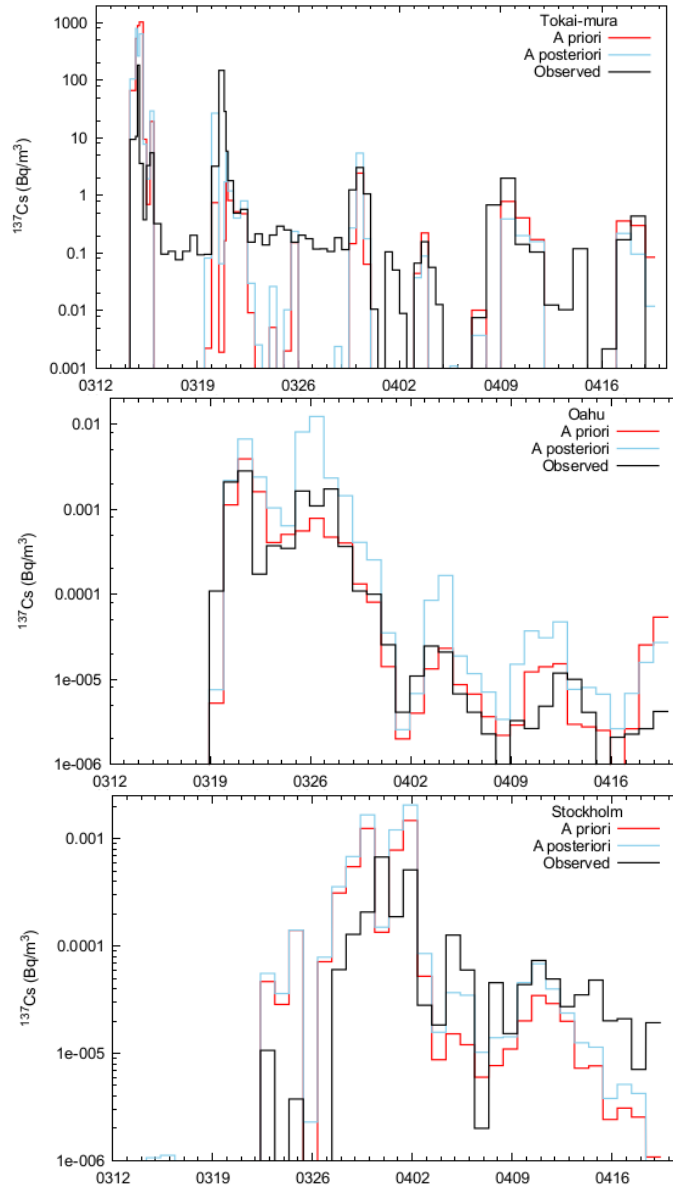


Figure 18: Measured Cs-137 concentrations, represented by black lines at the stations: Tokai-mura, Oahu (Hawaii) and Stockholm. Source: Stohl [19]. In addition, some results of the FLEXPART model are presented and marked with different colors.

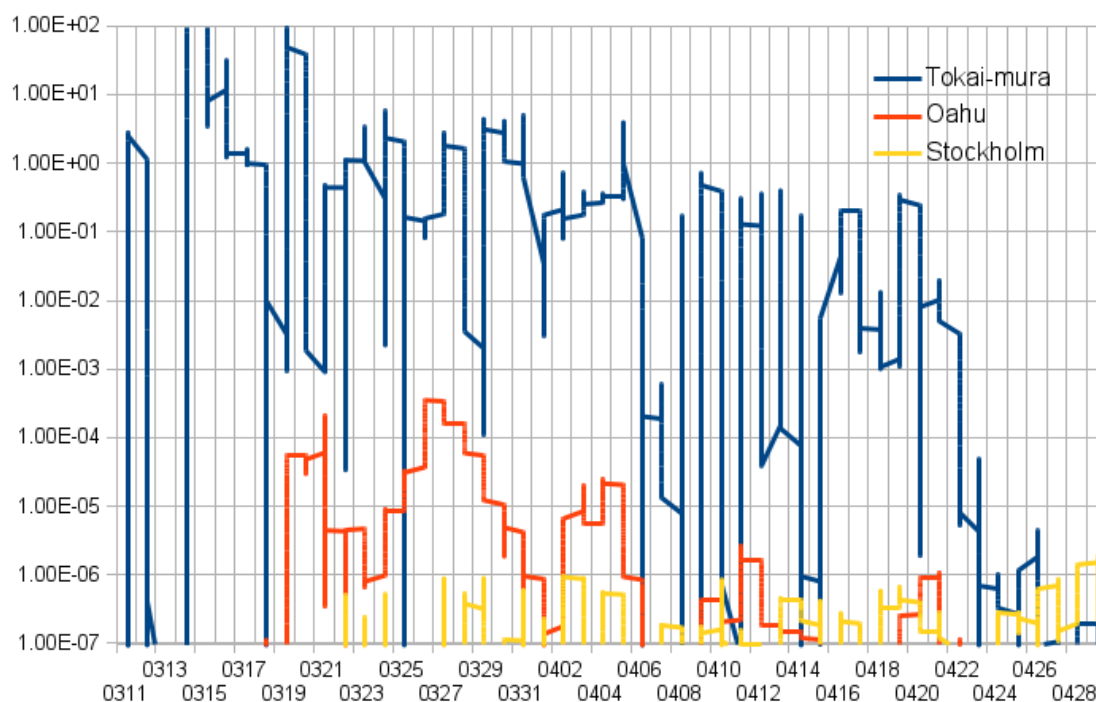


Figure 19: Time series of calculated with EEMEP model concentrations of Cs-137 for the stations Tokai-mura (blue line), Oahu (red line) and Stockholm (yellow line) after Fukushima accident.

Two maxima can be noticed in Cs-137 concentrations measured at Tokai-mura station. The first one is on 14 and the second on 19 March, both with the concentrations above  $100 \text{ Bq m}^{-3}$ . Throughout March and until 18 April, the measured concentrations are on the level of  $1 \text{ Bq m}^{-3}$  or slightly lower, but above  $0.1 \text{ Bq m}^{-3}$ . In the model calculations, the first significant peak can be seen also on 14 March and the second on 20 March, which means good correlation between the extreme values in measurements and model results. The EEMEP model predicts also higher concentration level already on 12 March, a bit earlier than measurements. This fact can be explained by a relatively large model grid size (ca. 150 km) and close location to the source of this site.

In the Oahu measurements, the concentration start to be visible on 19 March with increasing values until 21 March when the absolute maximum can be noticed above  $1.0 \times 10^{-3} \text{ Bq m}^{-3}$ . The next local maximum appears between 25 and 27 March with slightly lower values, but still above  $1.0 \times 10^{-3} \text{ Bq m}^{-3}$ . Later on, until 20 April, measured concentrations are lower, close to  $1.0 \times 10^{-5} \text{ Bq m}^{-3}$ . The EEMEP predicts the same arrival time on 19 March, but the initial concentration is slightly lower -  $1.0 \times 10^{-4} \text{ Bq m}^{-3}$ . Also the second measured maximum on 25 March is well reproduced by the EEMEP model, but calculated concentrations are again lower than measured by one order of magnitude. The EEMEP model shows some low

#### 4. Preliminary comparison of model results with measurements

( $1.0 \times 10^{-6}$  Bq m<sup>-3</sup>) concentrations for the rest of March and until 22 April, which is in agreement with measurements.

The significant concentrations measured in Stockholm appear as small ( $1.0 \times 10^{-5}$  Bq m<sup>-3</sup>) individual peaks on 23 and 25 of March. Starting from 28 March, the measured concentrations begin to increase rapidly reaching the maxima on 30 March and 1 April, both close to 0.001 Bq m<sup>-3</sup>. Later on, until 20 April, the measured concentrations remain close to  $1.0 \times 10^{-4}$  Bq m<sup>-3</sup> or slightly below. The EEMEP model predicts first significant concentrations also on 23 March, indicating a good agreement with measurements. However, the modelled concentrations for the entire period until 28 April are lower than measured, close or slightly below  $1.0 \times 10^{-6}$  Bq m<sup>-3</sup>.

In addition to three measurements sites from Stohl, we have also used the measurement data from one Norwegian station in Spitsbergen. These data include air concentrations of Cs-137 and were used for comparison with the EEMEP model results. The measurements from Spitsbergen were made available to us by NRPA.

In Fig. 20, the measured and modelled concentrations of Cs-137 are compared in the Spitsbergen station. There is a good agreement in measured and calculated arrival time, but calculated concentrations are at least one order of magnitude too low compared to measurements.

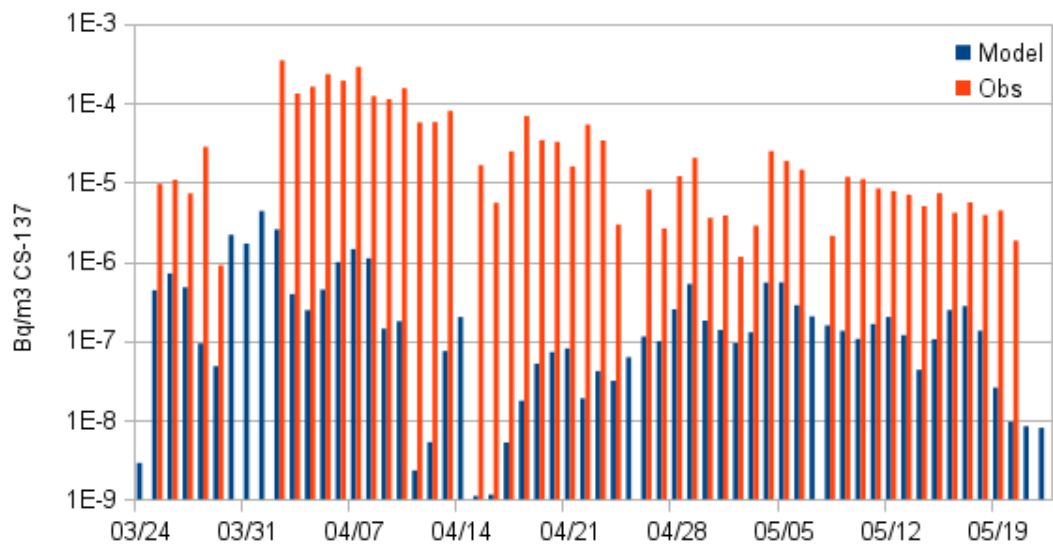


Figure 20: Comparison of model results and measurements in Spitsbergen for Cs-137 concentrations. Measurement data from NRPA.

At the current stage, the EEMEP model seems to slightly underestimate the measured concentrations in long range and long term atmospheric transport of radionuclides. The most likely reason of this underestimation is too efficient removal of radionuclides from the air in the processes of dry and mainly wet deposition. On the other hand, time of arrival is acceptable and



good considering a large model grid-size. This indicates a good description and parametrization of the transport and diffusion processes in the current version of the EEMEP model. However, this is only a preliminary comparison of the model results with measurements at this stage.

## 5. Model results in the ARGOS system

One of the main goals of the project is the implementation of an efficient and robust interface between the EEMEP model at MET and the ARGOS system at NRPA. Unfortunately, this is not possible in the first phase of the project. The results of the preliminary global EEMEP model are ready for the implementation into the ARGOS system, but the ARGOS system is not ready yet for receiving the results of the global run. This is mainly because of a very large size of the files to be transferred for the global scale simulations. Therefore, here we present a short description of the interface for regional model SNAP which is currently operational at MET and can be run remotely from NRPA. As soon as the ARGOS system is extended for the global scale, a very similar solution will be applied for the global EEMEP model.

Simulation of atmospheric dispersion of radioactive debris from nuclear accidents is the most important task of the operational dispersion models at MET. In fact, nuclear accident in Chernobyl in 1986 was the main reason for developing these models. A practical importance of this kind of modelling was confirmed by the nuclear accident in Fukushima in April 2011. Therefore, here we describe the remote application for nuclear accident as an example. This application is shown for the regional SNAP model [3], but the future application for the global EEMEP model will be very similar.

### 5.1. Computational scheme for nuclear accident

The sequence of events starts at NRPA in the frame of ARGOS system and is illustrated in Fig. 21 in the computational diagram for the accident case.

In the remote SNAP applications from NRPA, the SNAP run for the nuclear accident is initiated when the new input file for the nuclear accident appears on the MET server. This file is originally in .xml format, but it is converted to a simple text file at MET. A test example of such input file (NRPA-input.txt) is shown below.

```
57.249982262757 LATITUDE
12.0998963945262 LONGITUDE
2011-10-12T06:00:00Z RELEASE START
3 ISOTOPES
748 I -131a
158 Xe-133
169 Cs-137
2 RELEASE INTERVALS
INTERVAL
10 0 HOUR,MINUTE
10 45 RELEASE HEIGHT MIN,MAX
748 57667598327
158 44058874033996
169 5814817158
INTERVAL
5 0 HOUR,MINUTE
10 35 RELEASE HEIGHT MIN,MAX
748 5000000000
158 4000000000000
169 600000000
```

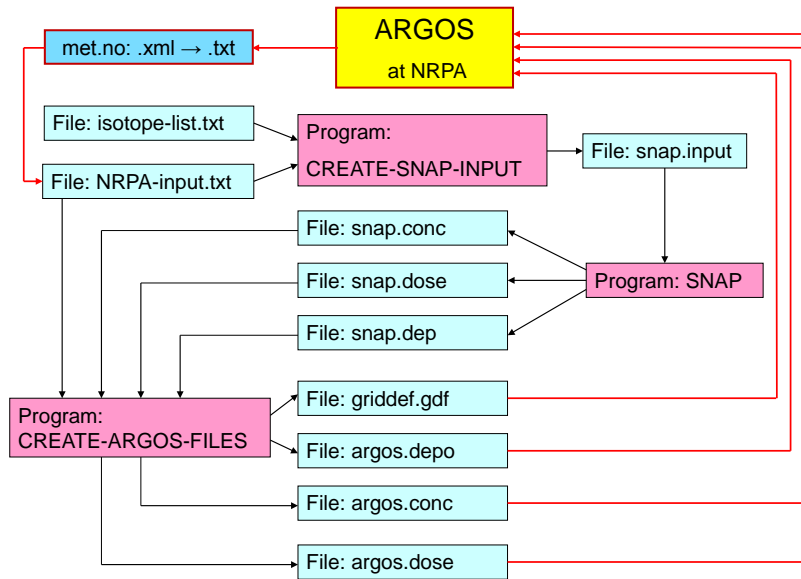


Figure 21: Computational diagram for the interface between SNAP and ARGOS at MET, for the accident case.

The first two lines of the file give the geographical co-ordinates of the accident and at the same time the release location. The third line specifies the date and time (in hours, minutes and seconds) of the accident and beginning of release. The fourth line gives the number of isotopes to be simulated. In this case, there are three isotopes with the identification numbers and names specified in three following lines and taken from the isotope list in Appendix A. Next line gives the total number of release intervals, which are two in this test case. In the first interval the release duration is 10 hours and 0 minutes. The minimum elevation of release is 10 m and maximum elevation of release is 45 m. Next three lines specify the release rate (in  $\text{Bq s}^{-1}$ ) for each simulated isotope with corresponding identification number. The duration of release in the second interval is 5 hours and 0 minutes with vertical range 10-35 m and there are also three different release rates for each isotope. They are specified in the last three lines of the file.

Two input files are necessary to start the SNAP run at MET: `NRPA-input.txt` and `isotope-list.txt`. The file `isotope-list.txt` is presented as a table in Appendix A. Altogether there are 382 isotopes listed in Appendix A which can be used in remote applications of SNAP from NRPA. The identification number of each isotope is given in the first column and name of the isotope in the second column. There can be three forms of the isotope denoted by a single digit number: 0-noble gas, 1-gas and 2-aerosol. This information is included in the third column. The decay coefficient ( $\text{s}^{-1}$ ) is given in column four.

Program `CREATE-SNAP-INPUT` (Fig. 21) is creating the input file (`snap.input`) for the SNAP model using the information included in the files: `NRPA-input.txt` and `isotope-list.txt`. Next step is the SNAP model run producing three intermediate output files:

## 5. Model results in the ARGOS system

`snap.conc`, `snap.dose` and `snap.dep`, including calculated instantaneous concentrations, time integrated concentrations and deposition, respectively. These files are very large, because they contain many unnecessary zeros in the model grid system. The intermediate output files are then converted to final output files by program `CREATE-ARGOS-FILES`. The final output files are much smaller because they include only non-zero values of concentration and deposition. Program `CREATE-ARGOS-FILES` is also producing an additional file `isotope-griddef.gdf` with model grid definition in geographical coordinates. The final output files are sent to the ARGOS system at NRPA as soon as they are created.

### 5.2. An example of remote application for nuclear accident

An example of the remote application from NRPA for nuclear accident is shown in Fig. 22 and Fig. 23. In this example atmospheric dispersion of radioactive debris from hypothetical accident in Ringhals (Sweden) nuclear power plant has been simulated. The start of the accident was assumed on 24 September 2011 at 13:00 UTC. Two isotopes Cs-137 and I-131 were released into the air for the period of 10 hours. Both isotopes were released into the abstract cylinder with the base at 10 m and top at 20 m. The cylinder radius was 20 m. The SNAP simulation of this accident was performed for 63 hours. The final results of the model run were available on 27 September 2011 at 04:00 UTC.

In Fig. 22 the results of SNAP simulation (time integrated concentration and deposition of I-131) are shown using the graphics available at MET. The radioactive debris from this accident is mainly transported and deposited over Swedish territory, reaching a small area of Northern Norway at the end of the simulation. There is also a small part of Southern Norway affected at the beginning of the transport. The range of the deposition is longer than the range of time integrated concentration, because a part of the radioactivity is transported higher in the air. It means zero concentration on the ground, but still possible wet deposition. In this case, the wet deposition process above the ground is quite effective, showing relatively high deposition values far away from the source in Northern Sweden, where time integrated concentrations were equal to zero. Both in the concentration and deposition maps, but especially in the deposition maps, two separate plums can be seen corresponding to different periods of the transport. The earlier tang is going south and then east whereas the later tang is going first south-north for a short period and then to the north.

In Fig. 23, the same results as in Fig. 22 are illustrated using the ARGOS graphics. Both, maps created at `met.no` and those in ARGOS system are very similar, however more details are visible on the ARGOS maps. The spatial distributions, as well as the gradients are very similar on the `met.no`'s and NRPA's maps.

5.2. An example of remote application for nuclear accident

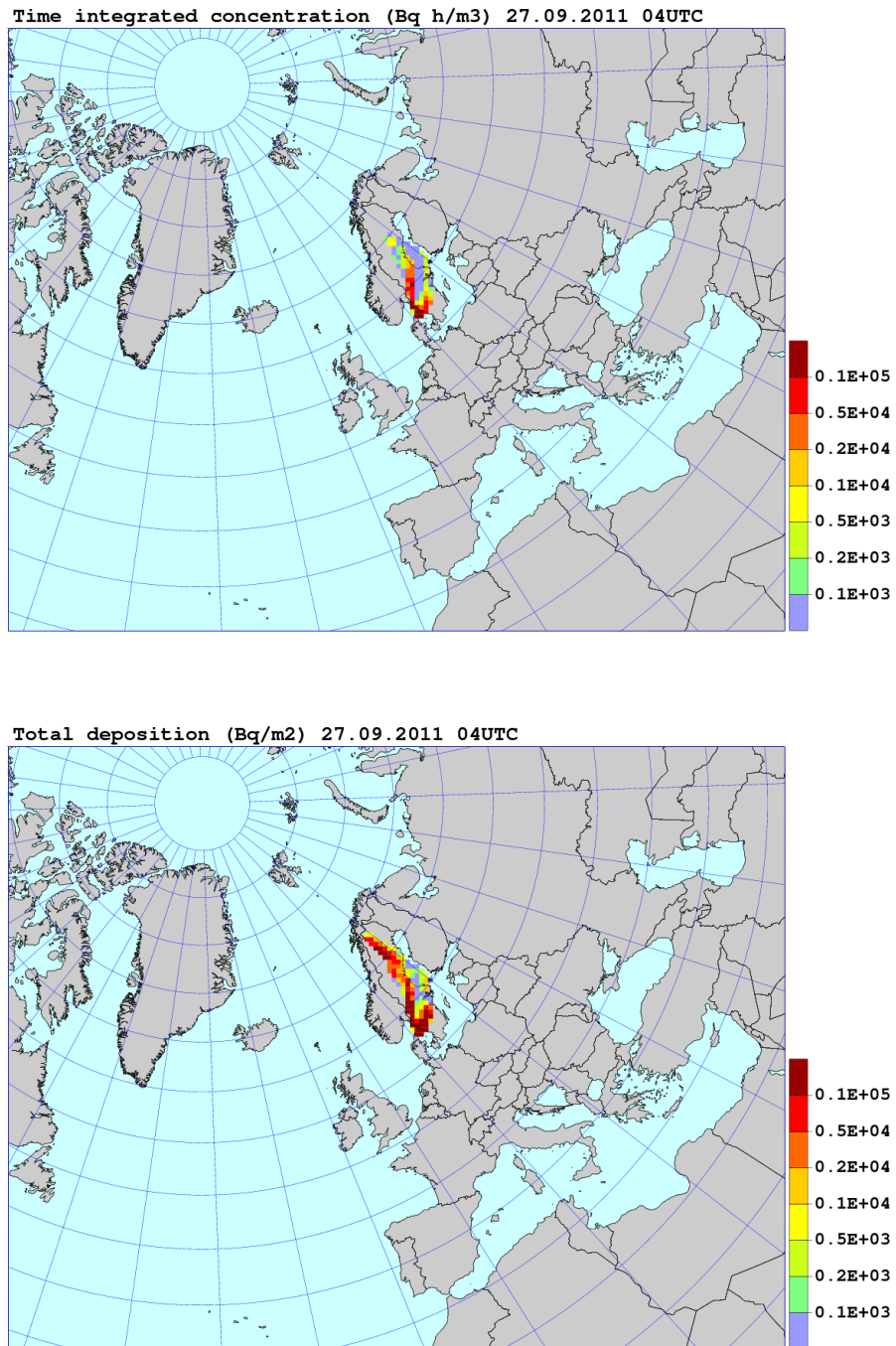


Figure 22: Maps of time integrated I-131 concentration (above) and total deposition (below). Results of SNAP run performed at MET for the test accident submitted by NRPA.

## 5. Model results in the ARGOS system

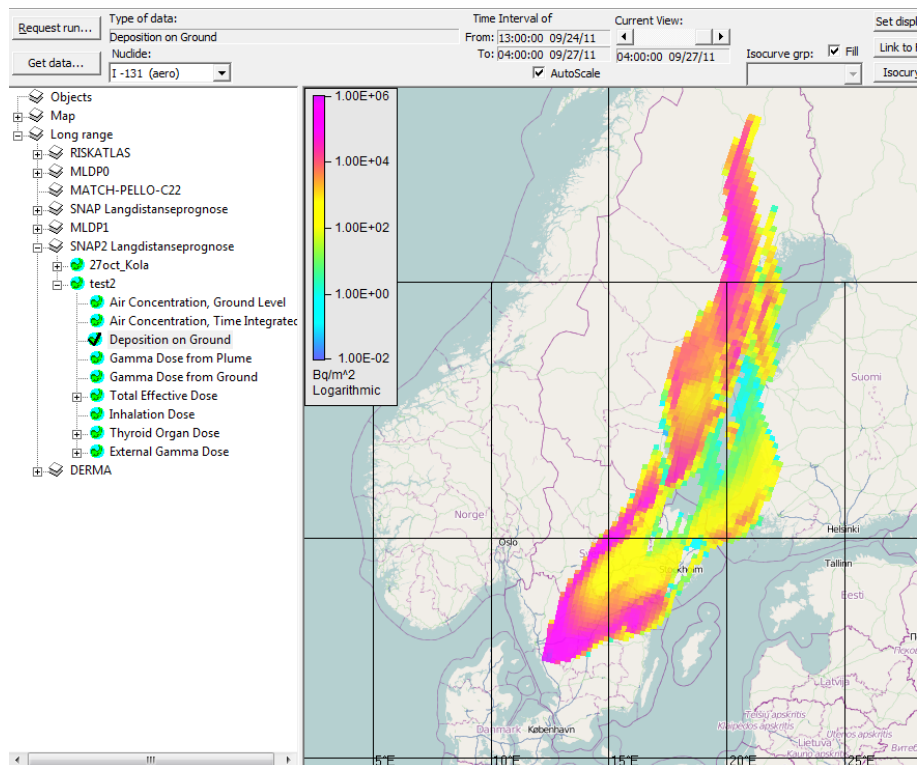
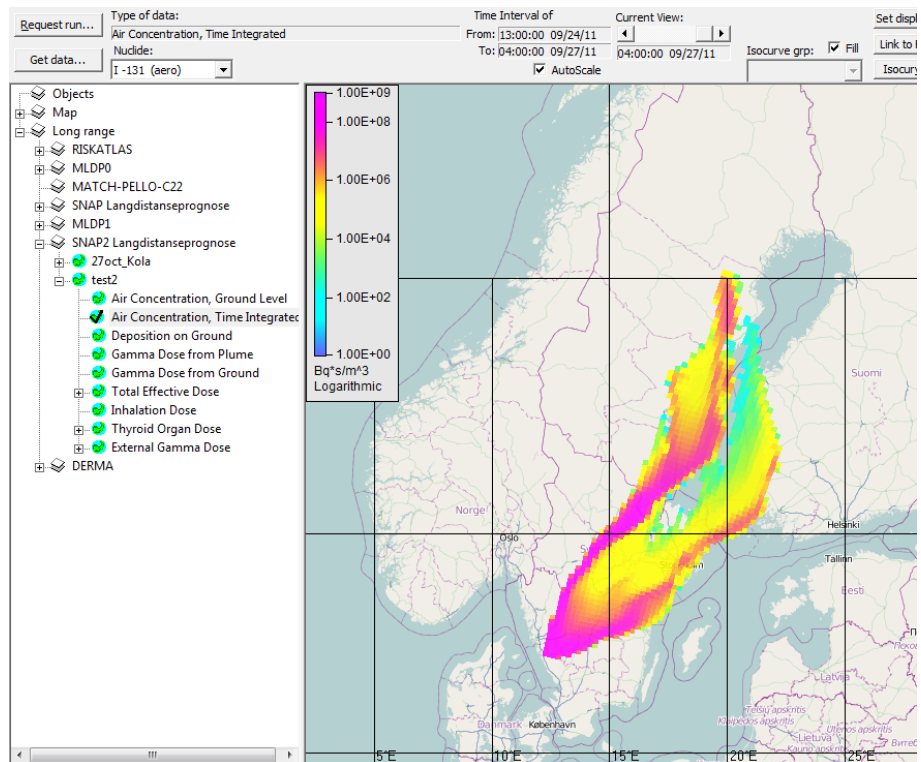


Figure 23: Screen dumps of the time integrated I-131 concentration (above) and deposition (below) from the test accident run post processed in the ARGOS system at NRPA. Results of the same SNAP run as presented in Fig. 22.

## 6. Conclusions

The main goal of this phase of the project was a development of a preliminary version of the Eulerian dispersion model for radioactive debris, which could be run in operational mode at MET. Such a preliminary version of the Eulerian EEMEP model has been developed and tested at MET within the project framework. The present model version operates in the global scale and can be used for simulating nuclear accident or explosion in arbitrary location on Earth. We call this version preliminary, because it is based on the EMEP MSC-W model. The EMEP MSC-W model was developed mainly for acidifying and eutrophying compounds and belongs to the group of CTM models. Therefore the EEMEP model requires further improvements specific for atmospheric transport and deposition of radionuclides with properties quite different from the compounds taken into account in the EMEP MSC-W model. Based on the work done within the project, the following conclusions can be formulated:

- Although preliminary, the current version of the EEMEP model is used as test-operational every day (at 00 and 12 UTC) at MET, for simulating hypothetical nuclear accidents and explosions in selected locations world-wide. The results of test-operational applications of EEMEP model up to now indicate that it can be a very useful forecasting tool for real emergency situations. It should be implemented as fully operational at MET in the future.
- The test runs of the EEMEP model with very long releases (one month and 6 weeks) of radionuclides from Fukushima reactors were performed in this phase of the project. They proved that the Eulerian model can be efficiently used in case of an accident with a long release. This is a very important feature and advantage of the Eulerian approach compared to Lagrangian modelling for which the source with a long term release of radionuclides is a real challenge.
- The results of the EEMEP runs for Fukushima accident were preliminary compared with the measurements. Unfortunately not too many of them were used, because only measurements at four stations were available for the comparison. This comparison, showed that dynamics in the model is well described and the calculated and observed time of arrival agrees very well for the long range transport. This agreement is not so good for the local measurements, because of a relatively large grid size (ca. 300 km) of the EEMEP model. Concerning concentration levels, the EEMEP model typically underestimates the measured concentrations. The most likely reason for the underestimation is too efficient parametrization of the deposition processes in the EEMEP model. This parametrization needs improvement and better adjustment to processes specific for radioactive substances. A more extensive comparison of the EEMEP model results with available measurements is necessary for model verification. It is planned for the second phase of the PREPARE project.
- One of other important goals of the project is a development of the interface between the results of the EEMEP model at MET and the ARGOS system at NRPA. This interface is currently operational for the regional SNAP model at MET, but cannot be extended for

## 6. Conclusions

the EEMEP model now, because such an extension for the global scale requires internal changes in the ARGOS system. As soon as the ARGOS system is ready, we will start to test the interface for the EEMEP model.

A general conclusion from the work done within the project is that the application of Eulerian model for simulation of atmospheric transport and deposition of radionuclides in the global scale is very promising. However, the present version of the EEMEP model needs further improvements. First of all, a better parametrization of the source terms for nuclear accident and explosion is needed in the Eulerian framework. Next, the EEMEP model needs a better and more detailed parametrization of dry and wet deposition processes. These improvements will be implemented in the second phase of the project.



## References

- [1] Bartnicki, J. and J. Saltbones (1996) Severe Nuclear Accident Program (SNAP) - A real time dispersion model. In: *Development and Application of Computer Techniques to Environmental Studies VI*. (P. Zannetti and C.A. Brebbia, eds.), pp. 17-26. Computational Mechanics Publications, Southampton, Boston.
- [2] Bartnicki J., B. Salbu, J. Saltbones, A. Foss and O. Ch. Lind (2003) Long-range transport of large particles in case of nuclear accident or explosion. Preprints of 26th NATO/CCMS International Technical Meeting on Air Pollution Modelling and its Application, 26-30 May 2003. Istanbul Technical University, Istanbul, Turkey, pp. 53-60.
- [3] Bartnicki J., H. Haakenstad and Ø. Hov (2013) Operational SNAP Model for Remote Applications From NRPA. MET Research Report No. 12/2013. Norwegian Meteorological Institute, Oslo, Norway.
- [4] Berglen, T., Berntsen, T., Isaksen, I., and Sundet, J. (2004) A global model of the coupled sulfur/oxidant chemistry in the troposphere: The sulfur cycle, *J. Geophys. Res.*, 109, D19310, doi:10.1016/j.atmosenv.2004.02.034.
- [5] Bott A. (1989a) A positive definite advection scheme obtained by non-linear re-normalization of the advection fluxes. *Mon. Weather Rev.*, 117:1006-1015.
- [6] Bott A. (1989b) Reply. *Mon. Weather Rev.*, 117:2633-2636.
- [7] Gallagher, M. W., Beswick, K. M., Duyzer, J., Westrate, H., Choularton, T. W., and Hummelshoj, P. (1997) Measurements of aerosol fluxes to Speulder forest using a micrometeorological technique, *Atmos. Environ.*, 31, 359-373.
- [8] Henzing, J. S., Olivie, D. J. L., and van Velthoven, P. F. J. (2006) A parameterization of size re-solved below cloud scavenging of aerosols by rain, *Atmos. Chem. Phys.*, 6, 3363-3375, doi:10.5194/acp-6-3363-2006.
- [9] Laakso, L., Gronholm, T., Rannik, U., Kosmale, M., Fiedler, V., Vehkamäki, H., and Kulmala, M. (2003) Ultrafine particle scavenging coefficients calculated from 6 years field measurements, *Atmos. Environ.*, 37, 3605-3613, 2003.
- [10] Persson Ch., Robertson L. and Thaning L. (2000) Model Simulation of Air and Ground Contamination Associated with Nuclear Weapons. An Emergency Preparedness Model. SMHI report No 95. Swedish Meteorological and Hydrological Institute. Norrköping, Sweden.
- [11] Saltbones J. (1995) Real-time dispersion model calculations as part of NORMEM-WP19. *Safety Science* 20, 51-59.
- [12] Saltbones J., Foss A. and J. Bartnicki (1995) Severe Nuclear Accident Program. Technical Description. Research Report No. 15. Norwegian Meteorological Institute. Oslo, Norway.

## References

- [13] Saltbones J., Foss A. and J. Bartnicki (1995) Severe Nuclear Accident Program (SNAP) - A real time dispersion model. In: Proceedings of Oslo Conference on International Aspects of Emergency management and Environmental Technology. (K.H. Drager ed.), pp. 177-184.
- [14] Saltbones J., Bartnicki J. and A. Foss (2003) Handling of Fallout Processes from Nuclear Explosions in Severe Nuclear Accident Program - SNAP. Research Report No. 157. Norwegian Meteorological Institute. Oslo, Norway.
- [15] Scott, B. C. (1979) Parameterization of sulphate removal by precipitation, *J. Appl. Met.*, 17, 11375-11389, 1979.
- [16] Simpson, D., Benedictow, A., Berge, H., Bergström, R., Emberson, L. D., Fagerli, H., Hayman, G. D., Gauss, M., Jonson, J. E., Jenkin, M. E., NyÅri, A., Richter, C., Semeena, V. S., Tsyro, S., Tuovinen, J.-P., Valdebenito, A., and Wind, P. (2012a) The EMEP MSC-W chemical transport model - Part 1: Model description, *Atmos. Chem. Phys. Discuss.*, 12, 3781-3874, doi:10.5194/acpd-12-3781-2012.
- [17] Simpson, D., A. Benedictow, H. Berge, R. Bergström, L. D. Emberson, H. Fagerli, C. R. Flechard, G. D. Hayman, M. Gauss, J. E. Jonson, M. E. Jenkin, A. NyÅri, C. Richter, V. S. Semeena, S. Tsyro, J.-P. Tuovinen, A. Valdebenito, and P. Wind (2012b) The EMEP MSC-W chemical transport model - technical description *Atmos. Chem. Phys.*, 12 (16), 7825-7865.
- [18] Stevenson, D., Dentener, F., Schultz, M., Ellingsen, K., van Noije, T., Wild, O., Zeng, G., Amann, M., Atherton, C., Bell, N., Bergmann, D., Bey, I., Butler, T., Cofala, J., Collins, W., Derwent, R., Doherty, R., Drevet, J., Eskes, H., Fiore, A., Gauss, M., Hauglustaine, D., Horowitz, L., Isaksen, I., Krol, M., Lamarque, J., Lawrence, M., Montanaro, V., Müller, J., Pitari, G., Prather, M., Pyle, J., Rast, S., Rodriguez, J., Sanderson, M., Savage, N., Shindell, D., Strahan, S., Sudo, K., and Szopa, S. (2006) Multimodel ensemble simulations of present-day and near-future tropospheric ozone, *J. Geophys. Res.*, 111, D08301, doi:10.1029/2005JD006338.
- [19] Stohl, A., P. Seibert, G. Wotawa, D. Arnold, J. F. Burkhart, S. Eckhardt, C. Tapia, A. Vargas and T. J. Yasunari (2012) Xenon-133 and caesium-137 releases into the atmosphere from the Fukushima Dai-ichi nuclear power plant: determination of the source term, atmospheric dispersion, and deposition, *Atmos. Chem. Phys.*, 12, 2313-2343.
- [20] Tiedtke, M. (1989) A Comprehensive Mass Flux Scheme For Cumulus Parameterization In Large-Scale Models, *Mon. Weather Rev.*, 117, 1779-1800.
- [21] Undén, P., Rontu, L., Järvinen, H., Lynch, P., Calvo, J., Cats, G., Cuaxart, J., Eerola, K., Fortelius, C., Garcia-Moya, J.A., Jones, C., Lenderlink, G., McDonald, A., McGrath, R., Navascues, B., Nielsen, N.W., Ødegaard, V., Rodriguez, E., Rummukainen, M., Rööm, R., Sattler, K., Sass, B.H., Savijärvi, H., Schreur, B.W., Sigg, R., The, H. and Tijn, A. (2002) HIRLAM-5 Scientific Documentation, HIRLAM-5 Project. Available from SMHI, S-601767 Norrköping, Sweden.

- [22] Venkatram, A. and J. Pleim, (1999) The electrical analogy does not apply to modeling dry deposition of particles, *Atmos. Environ.*, 33, 3075-3076.
- [23] Wesely, M. L., Cook, D. R., Hart, R. L., and Speer, R. E. (1985) Measurements and Parameterization of Particulate Sulfur Dry Deposition over Grass, *J. Geophys. Res.*, 90, 2131-2143.

## A. List of isotopes for EEMEP simulations

In this Appendix we show the list of isotopes important for NRPA which can be used in EEMEP simulations. Altogether there are 382 isotopes. Identification number of each isotope is given in the first column and name of the isotope in the second column. There can be three forms of the isotope specified by one digit number: 0-noble gas, 1-gas and 2-aerosol. This information is included in the third column. The radioactive decay constant is given in column four with the unit  $s^{-1}$ .

Identification number	Name	Type	Decay constant
1	H - 3	0	0.178E-08
2	Na- 24	2	0.128E-04
3	Ar- 41	0	0.105E-03
4	Co- 58	2	0.113E-06
5	Co- 60	2	0.416E-08
6	Zn- 72	2	0.414E-05
7	Ga- 72	2	0.137E-04
8	Ga- 73	2	0.395E-04
9	Ge- 75	2	0.140E-03
10	Ge- 77m	2	0.128E-01
11	Ge- 77	2	0.170E-04
12	Ge- 78	2	0.133E-03
13	As- 77	2	0.496E-05
14	As- 78	2	0.127E-03
15	Se- 79	2	0.338E-12
16	Se- 81m	2	0.202E-03
17	Se- 81	2	0.625E-03
18	Se- 83m	2	0.990E-02
19	Se- 83	2	0.513E-03
20	Br- 82m	2	0.189E-02
21	Br- 82	2	0.544E-05
22	Br- 83	2	0.802E-04
23	Br- 84m	2	0.193E-02
24	Br- 84	2	0.363E-03
25	Kr- 83m	0	0.104E-03
26	Kr- 85m	0	0.438E-04
27	Kr- 85	0	0.203E-08
28	Kr- 87	0	0.152E-03
29	Kr- 88	0	0.686E-04
30	Kr- 89	0	0.364E-02

Identification number	Name	Type	Decay rate
31	Rb- 86m	2	0.114E-01
32	Rb- 86	2	0.430E-06
33	Rb- 87	2	0.470E-18
34	Rb- 88	2	0.642E-03
35	Rb- 89	2	0.760E-03
36	Sr- 89	2	0.154E-06
37	Sr- 90	2	0.787E-09
38	Sr- 91	2	0.203E-04
39	Sr- 92	2	0.711E-04
40	Y - 90m	2	0.604E-04
41	Y - 90	2	0.301E-05
42	Y - 91m	2	0.232E-03
43	Y - 91	2	0.137E-06
44	Y - 92	2	0.545E-04
45	Y - 93	2	0.189E-04
46	Y - 94	2	0.608E-03
47	Y - 95	2	0.110E-02
48	Zr- 93	2	0.231E-13
49	Zr- 95	2	0.123E-06
50	Zr- 97	2	0.115E-04
51	Nb- 94m	2	0.185E-02
52	Nb- 94	2	0.110E-11
53	Nb- 95m	2	0.222E-05
54	Nb- 95	2	0.228E-06
55	Nb- 96	2	0.823E-05
56	Nb- 97m	2	0.128E-01
57	Nb- 97	2	0.157E-03
58	Nb- 98	2	0.227E-03
59	Mo- 99	2	0.289E-05
60	Mo-101	2	0.791E-03
61	Mo-102	2	0.104E-02
62	Tc- 99m	2	0.320E-04
63	Tc- 99	2	0.103E-12
64	Tc-101	2	0.814E-03
65	Tc-102m	2	0.269E-02
66	Tc-102	2	0.131E+00
67	Tc-104	2	0.642E-03
68	Ru-103	2	0.203E-06
69	Ru-105	2	0.434E-04
70	Ru-106	2	0.219E-07

A. List of isotopes for EEMEP simulations

Identification number	Name	Type	Decay rate
71	Rh-103m	2	0.206E-03
72	Rh-105m	2	0.182E-01
73	Rh-105	2	0.542E-05
74	Rh-106m	2	0.883E-04
75	Rh-106	2	0.232E-01
76	Rh-107	2	0.532E-03
77	Pd-107m	2	0.325E-01
78	Pd-107	2	0.338E-14
79	Pd-109	2	0.143E-04
80	Pd-111m	2	0.350E-04
81	Pd-111	2	0.525E-03
82	Pd-112	2	0.958E-05
83	Ag-109m	2	0.175E-01
84	Ag-110m	2	0.297E-07
85	Ag-111m	2	0.937E-02
86	Ag-111	2	0.107E-05
87	Ag-112	2	0.615E-04
88	Ag-113m	2	0.105E-01
89	Ag-113	2	0.363E-04
90	Ag-115m	2	0.408E-01
91	Ag-115	2	0.550E-03
92	Cd-111m	2	0.237E-03
93	Cd-113m	2	0.151E-08
94	Cd-113	2	0.244E-23
95	Cd-115m	2	0.180E-06
96	Cd-115	2	0.360E-05
97	Cd-117m	2	0.566E-04
98	Cd-117	2	0.741E-04
99	Cd-118	2	0.230E-03
100	In-113m	2	0.116E-03
101	In-115m	2	0.428E-04
102	In-115	2	0.431E-23
103	In-116m	2	0.213E-03
104	In-116	2	0.488E-01
105	In-117m	2	0.993E-04
106	In-117	2	0.263E-03
107	In-118m	2	0.263E-02
108	In-118	2	0.139E+00
109	In-119m	2	0.642E-03
110	In-119	2	0.462E-02

Identification number	Name	Type	Decay rate
111	Sn-117m	2	0.573E-06
112	Sn-119m	2	0.328E-07
113	Sn-121m	2	0.440E-09
114	Sn-121	2	0.718E-05
115	Sn-123m	2	0.289E-03
116	Sn-123	2	0.622E-07
117	Sn-125	2	0.831E-06
118	Sn-126	2	0.220E-12
119	Sn-127	2	0.908E-04
120	Sn-128	2	0.196E-03
121	Sn-130	2	0.312E-02
122	Sb-124m	2	0.569E-03
123	Sb-124	2	0.133E-06
124	Sb-125	2	0.805E-08
125	Sb-126m	2	0.608E-03
126	Sb-126	2	0.647E-06
127	Sb-127	2	0.211E-05
128	Sb-128m	2	0.111E-02
129	Sb-128	2	0.214E-04
130	Sb-129	2	0.444E-04
131	Sb-130m	2	0.175E-02
132	Sb-130	2	0.312E-03
133	Sb-131	2	0.502E-03
134	Te-125m	2	0.138E-06
135	Te-127m	2	0.736E-07
136	Te-127	2	0.205E-04
137	Te-129m	2	0.240E-06
138	Te-129	2	0.165E-03
139	Te-131m	2	0.642E-05
140	Te-131	2	0.462E-03
141	Te-132	2	0.247E-05
142	Te-133m	2	0.209E-03
143	Te-133	2	0.924E-03
144	Te-134	2	0.275E-03
145	I -129	1	0.138E-14
146	I -130m	1	0.130E-02
147	I -130	1	0.155E-04
148	I -131	1	0.994E-06
149	I -132	1	0.836E-04
150	I -133m	1	0.770E-01

A. List of isotopes for EEMEP simulations

Identification number	Name	Type	Decay rate
151	I -133	1	0.921E-05
152	I -134m	1	0.321E-02
153	I -134	1	0.222E-03
154	I -135	1	0.288E-04
155	Xe-129m	0	0.100E-05
156	Xe-131m	0	0.680E-06
157	Xe-133m	0	0.355E-05
158	Xe-133	0	0.152E-05
159	Xe-134m	0	0.239E+01
160	Xe-135m	0	0.743E-03
161	Xe-135	0	0.210E-04
162	Xe-137	0	0.296E-02
163	Xe-138	0	0.815E-03
164	Cs-134m	2	0.664E-04
165	Cs-134	2	0.107E-07
166	Cs-135m	2	0.218E-03
167	Cs-135	2	0.956E-14
168	Cs-136	2	0.617E-06
169	Cs-137	2	0.729E-09
170	Cs-138	2	0.359E-03
171	Ba-135m	2	0.671E-05
172	Ba-137m	2	0.453E-02
173	Ba-139	2	0.139E-03
174	Ba-140	2	0.627E-06
175	La-140	2	0.456E-05
176	La-141	2	0.498E-04
177	La-142	2	0.125E-03
178	La-143	2	0.825E-03
179	Ce-141	2	0.243E-06
180	Ce-142	2	0.440E-24
181	Ce-143	2	0.584E-05
182	Ce-144	2	0.282E-07
183	Ce-146	2	0.814E-03
184	Pr-142m	2	0.791E-03
185	Pr-142	2	0.101E-04
186	Pr-143	2	0.591E-06
187	Pr-144m	2	0.161E-02
188	Pr-144	2	0.669E-03
189	Pr-145	2	0.322E-04
190	Pr-146	2	0.477E-03



Identification number	Name	Type	Decay rate
191	Pr-147	2	0.963E-03
192	Nd-144	2	0.105E-22
193	Nd-147	2	0.730E-06
194	Nd-149	2	0.111E-03
195	Nd-151	2	0.932E-03
196	Nd-152	2	0.101E-02
197	Pm-147	2	0.838E-08
198	Pm-148m	2	0.194E-06
199	Pm-148	2	0.149E-05
200	Pm-149	2	0.363E-05
201	Pm-150	2	0.718E-04
202	Pm-151	2	0.678E-05
203	Pm-152m	2	0.642E-03
204	Pm-152	2	0.282E-02
205	Sm-147	2	0.205E-18
206	Sm-148	2	0.275E-23
207	Sm-149	2	0.220E-23
208	Sm-151	2	0.236E-09
209	Sm-153	2	0.414E-05
210	Sm-155	2	0.520E-03
211	Sm-156	2	0.205E-04
212	Eu-154	2	0.256E-08
213	Eu-155	2	0.458E-08
214	Eu-156	2	0.528E-06
215	Eu-157	2	0.127E-04
216	Eu-158	2	0.252E-03
217	Eu-159	2	0.638E-03
218	Gd-159	2	0.104E-04
219	Gd-162	2	0.116E-02
220	Tb-160	2	0.111E-06
221	Tb-161	2	0.116E-05
222	Tb-162m	2	0.863E-04
223	Tb-162	2	0.155E-02
224	Tb-163	2	0.592E-03
225	Dy-165	2	0.819E-04
226	Hg-206	2	0.144E-02
227	Tl-206	2	0.276E-02
228	Tl-207	2	0.241E-02
229	Tl-208	2	0.373E-02
230	Tl-209	2	0.525E-02

A. List of isotopes for EEMEP simulations

Identification number	Name	Type	Decay rate
231	Tl-210	2	0.889E-02
232	Pb-207m	2	0.866E+00
233	Pb-209	2	0.583E-04
234	Pb-210	2	0.105E-08
235	Pb-211	2	0.320E-03
236	Pb-212	2	0.181E-04
237	Pb-213	2	0.116E-02
238	Pb-214	2	0.431E-03
239	Bi-209	2	0.110E-25
240	Bi-210	2	0.160E-05
241	Bi-211	2	0.537E-02
242	Bi-212	2	0.191E-03
243	Bi-213	2	0.246E-03
244	Bi-214	2	0.586E-03
245	Bi-215	2	0.165E-02
246	Po-210	2	0.580E-07
247	Po-211	2	0.133E+01
248	Po-212	2	0.228E+07
249	Po-213	2	0.165E+06
250	Po-214	2	0.423E+04
251	Po-215	2	0.389E+03
252	Po-216	2	0.462E+01
253	Po-217	2	0.693E-01
254	Po-218	2	0.379E-02
255	At-215	2	0.693E+04
256	At-216	2	0.231E+04
257	At-217	2	0.217E+02
258	At-218	2	0.347E+00
259	At-219	2	0.128E-01
260	Rn-218	0	0.198E+02
261	Rn-219	0	0.173E+00
262	Rn-220	0	0.126E-01
263	Rn-221	0	0.462E-03
264	Rn-222	0	0.210E-05
265	Rn-223	0	0.269E-03
266	Fr-221	2	0.241E-02
267	Fr-222	2	0.781E-03
268	Fr-223	2	0.525E-03
269	Ra-222	2	0.182E-01
270	Ra-223	2	0.702E-06

Identification number	Name	Type	Decay rate
271	Ra-224	0	0.220E-05
272	Ra-225	0	0.542E-06
273	Ra-226	0	0.137E-10
274	Ra-227	0	0.280E-03
275	Ra-228	0	0.328E-08
276	Ra-229	0	0.693E+12
277	Ac-225	2	0.802E-06
278	Ac-226	2	0.664E-05
279	Ac-227	2	0.102E-08
280	Ac-228	2	0.314E-04
281	Ac-229	2	0.175E-03
282	Th-226	2	0.374E-03
283	Th-227	2	0.441E-06
284	Th-228	2	0.115E-07
285	Th-229	2	0.299E-11
286	Th-230	2	0.275E-12
287	Th-231	2	0.755E-05
288	Th-232	2	0.156E-17
289	Th-233	2	0.520E-03
290	Th-234	2	0.333E-06
291	Pa-230	2	0.453E-06
292	Pa-231	2	0.676E-12
293	Pa-232	2	0.612E-05
294	Pa-233	2	0.297E-06
295	Pa-234m	2	0.987E-02
296	Pa-234	2	0.285E-04
297	U -230	2	0.386E-06
298	U -231	2	0.187E-05
299	U -232	2	0.305E-09
300	U -233	2	0.136E-12
301	U -234	2	0.889E-13
302	U -235	2	0.309E-16
303	U -236	2	0.919E-15
304	U -237	2	0.119E-05
305	U -238	2	0.487E-17
306	U -239	2	0.492E-03
307	U -240	2	0.134E-04
308	Np-235	2	0.196E-07
309	Np-236m	2	0.170E-15
310	Np-236	2	0.875E-05

A. List of isotopes for EEMEP simulations

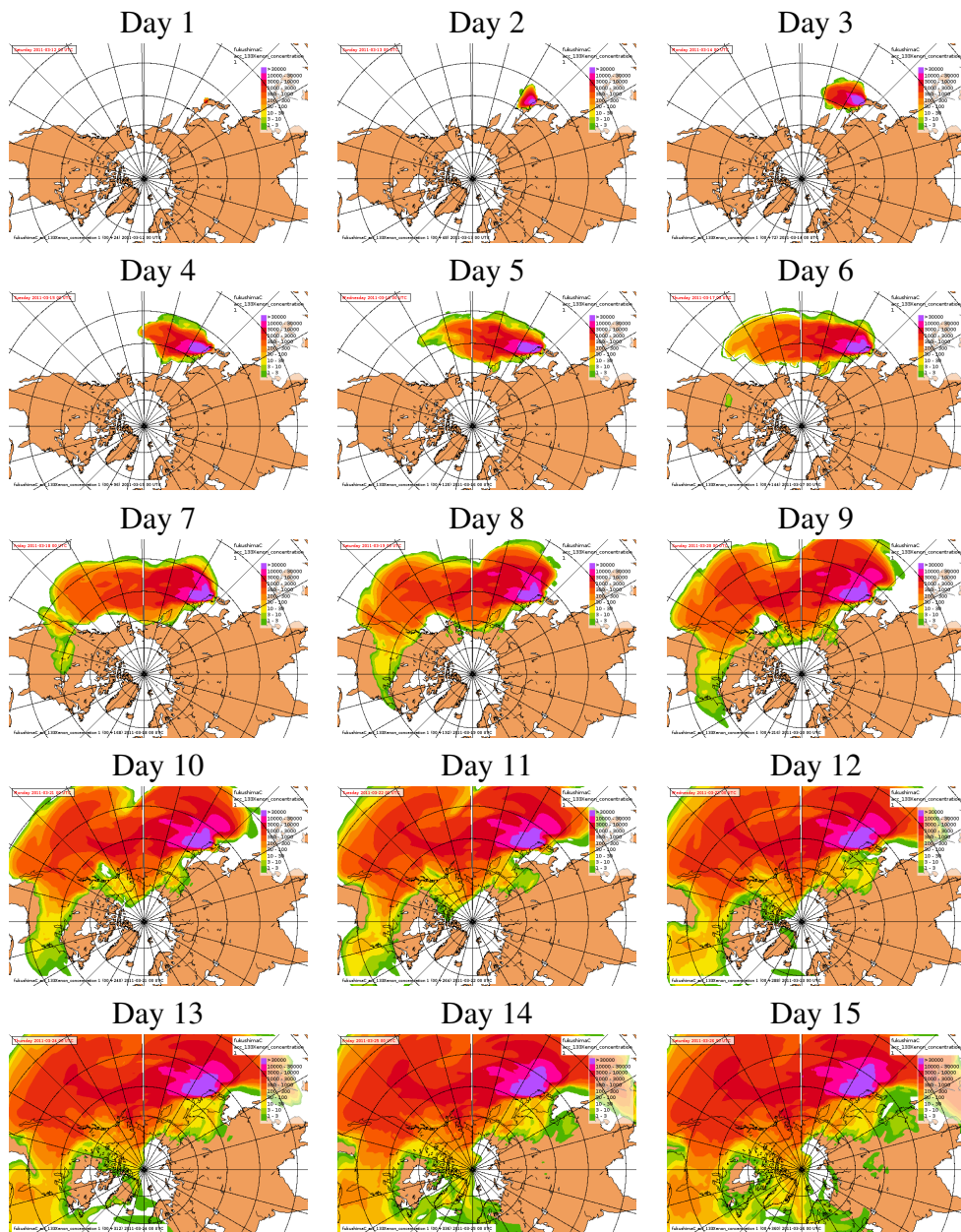
Identification number	Name	Type	Decay rate
311	Np-237	2	0.103E-13
312	Np-238	2	0.382E-05
313	Np-239	2	0.341E-05
314	Np-240m	2	0.158E-02
315	Np-240	2	0.183E-03
316	Pu-235	2	0.444E-03
317	Pu-236	2	0.771E-08
318	Pu-237	2	0.176E-06
319	Pu-238	2	0.255E-09
320	Pu-239	2	0.900E-12
321	Pu-240	2	0.334E-11
322	Pu-241	2	0.166E-08
323	Pu-242	2	0.580E-13
324	Pu-243	2	0.387E-04
325	Pu-244	2	0.275E-15
326	Pu-245	2	0.193E-04
327	Am-240	2	0.378E-05
328	Am-241	2	0.480E-10
329	Am-242	2	0.495E+02
330	Am-242m	2	0.145E-09
331	Am-242	2	0.120E-04
332	Am-243	2	0.276E-11
333	Am-244m	2	0.444E-03
334	Am-244	2	0.191E-04
335	Am-245	2	0.917E-04
336	Cm-241	2	0.229E-06
337	Cm-242	2	0.492E-07
338	Cm-243	2	0.686E-09
339	Cm-244	2	0.125E-08
340	Cm-245	2	0.236E-11
341	Cm-246	2	0.399E-11
342	Cm-247	2	0.137E-14
343	Cm-248	2	0.467E-13
344	Cm-249	2	0.181E-03
345	Cm-250	2	0.318E-11
346	Bk-249	2	0.255E-07
347	Bk-250	2	0.598E-04
348	Cf-249	2	0.610E-10
349	Cf-250	2	0.169E-08
350	Cf-251	2	0.275E-10

Identification number	Name	Type	Decay rate
351	Cf-252	2	0.829E-08
352	Cf-253	2	0.456E-06
353	Cf-254	2	0.133E-06
354	Es-253	2	0.392E-06
355	Es-254m	2	0.491E-05
356	Es-254	2	0.291E-07
357	Es-255	2	0.209E-06
358	C - 11	0	0.567E-03
359	N - 13	0	0.116E-02
360	O - 15	0	0.567E-02
361	F - 18	0	0.115E-03
545	I -129e	1	0.138E-14
645	I -129o	1	0.138E-14
745	I -129a	1	0.138E-14
547	I -130e	1	0.155E-04
647	I -130o	1	0.155E-04
747	I -130a	1	0.155E-04
548	I -131e	1	0.994E-06
648	I -131o	1	0.994E-06
748	I -131a	1	0.994E-06
549	I -132e	1	0.836E-04
649	I -132o	1	0.836E-04
749	I -132a	1	0.836E-04
551	I -133e	1	0.921E-05
651	I -133o	1	0.921E-05
751	I -133a	1	0.921E-05
553	I -134e	1	0.222E-03
653	I -134o	1	0.222E-03
753	I -134a	1	0.222E-03
554	I -135e	1	0.288E-04
654	I -135o	1	0.288E-04
754	I -135a	1	0.288E-04

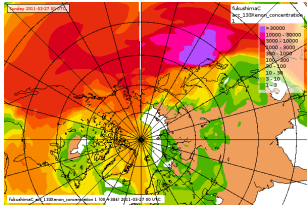
## B. Daily results of EEMEP run with one month release

In this Appendix we show the results of the EEMEP model run with a long release - one month. The daily maps of time integrated concentrations of Xe-133 and Cs-137 are presented. Units:  $\text{Bq h m}^{-3}$ .

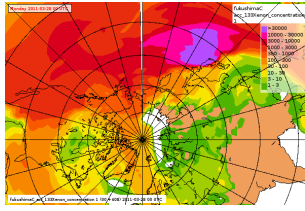
### Results for Xe-133. Days: 1-31



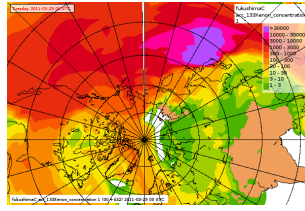
Day 16



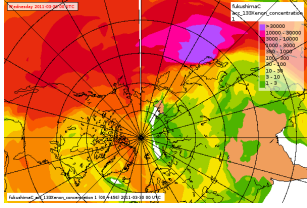
Day 17



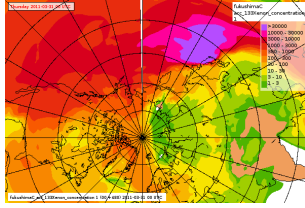
Day 18



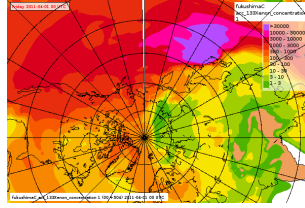
Day 19



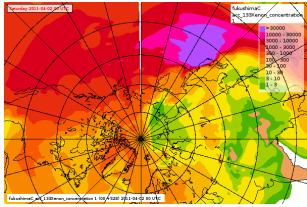
Day 20



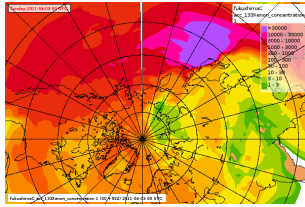
Day 21



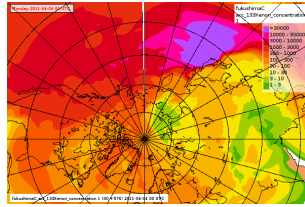
Day 22



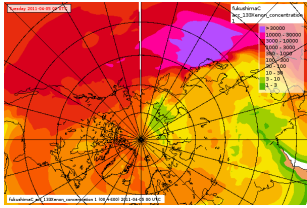
Day 23



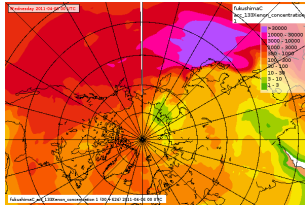
Day 24



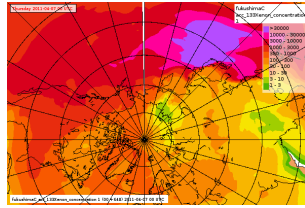
Day 25



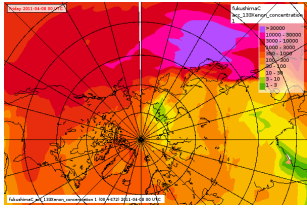
Day 26



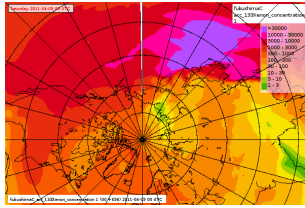
Day 27



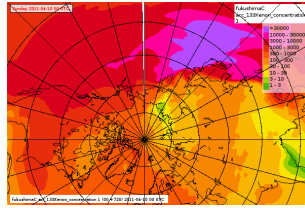
Day 28



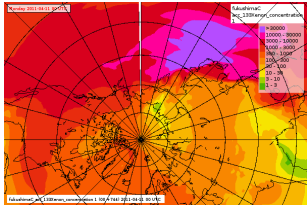
Day 29



Day 30

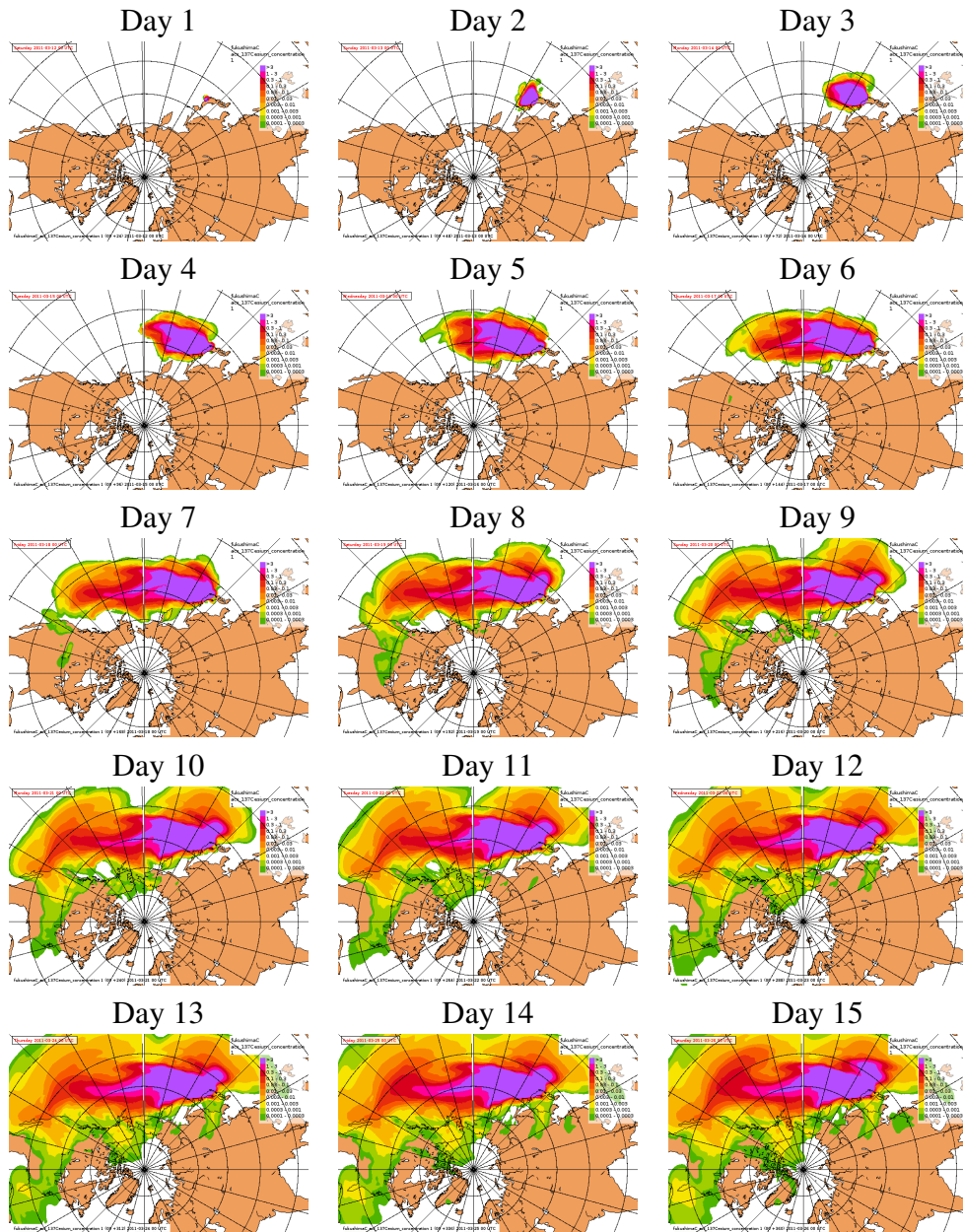


Day 31



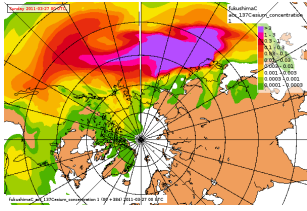
B. Daily results of EEMEP run with one month release

Results for Cs-137. Days: 1-31

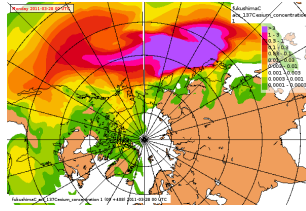




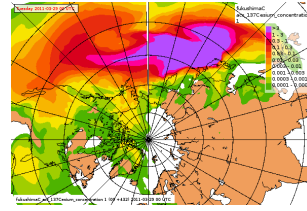
Day 16



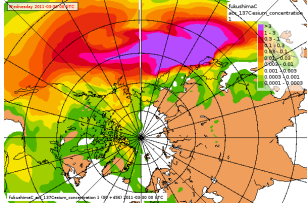
Day 17



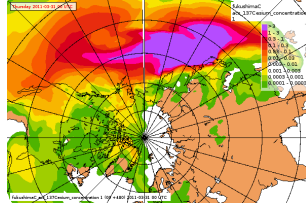
Day 18



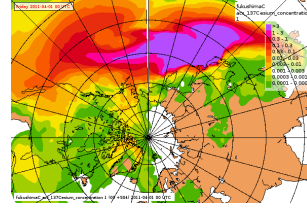
Day 19



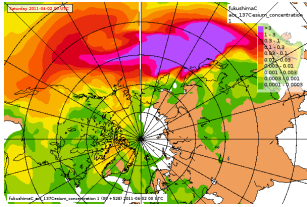
Day 20



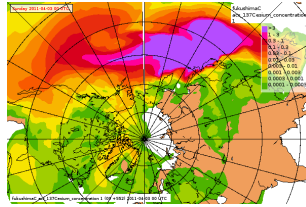
Day 21



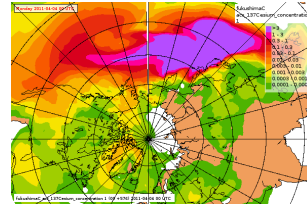
Day 22



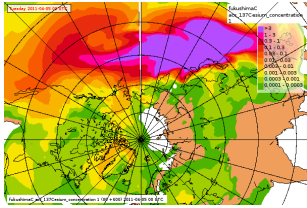
Day 23



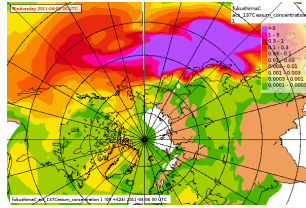
Day 24



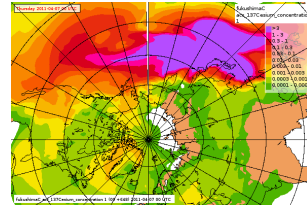
Day 25



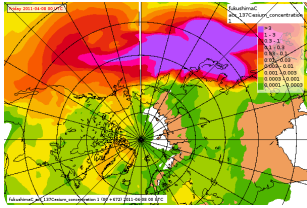
Day 26



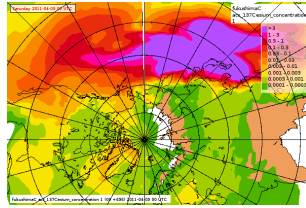
Day 27



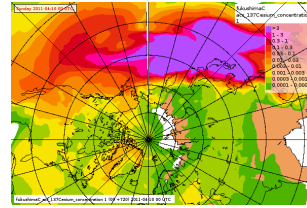
Day 28



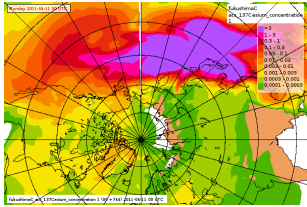
Day 29



Day 30



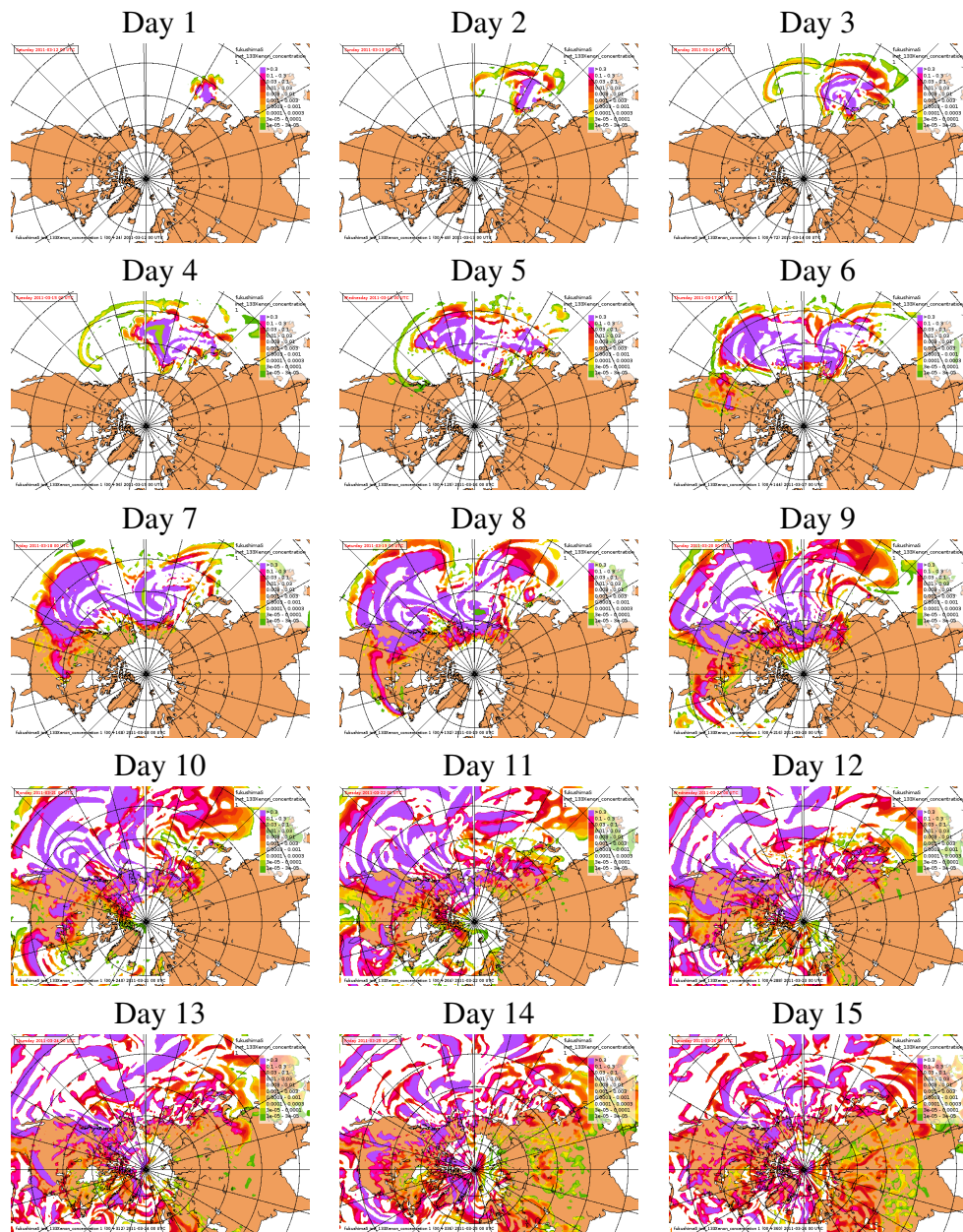
Day 31



## C. Daily results of EEMEP run with six weeks release

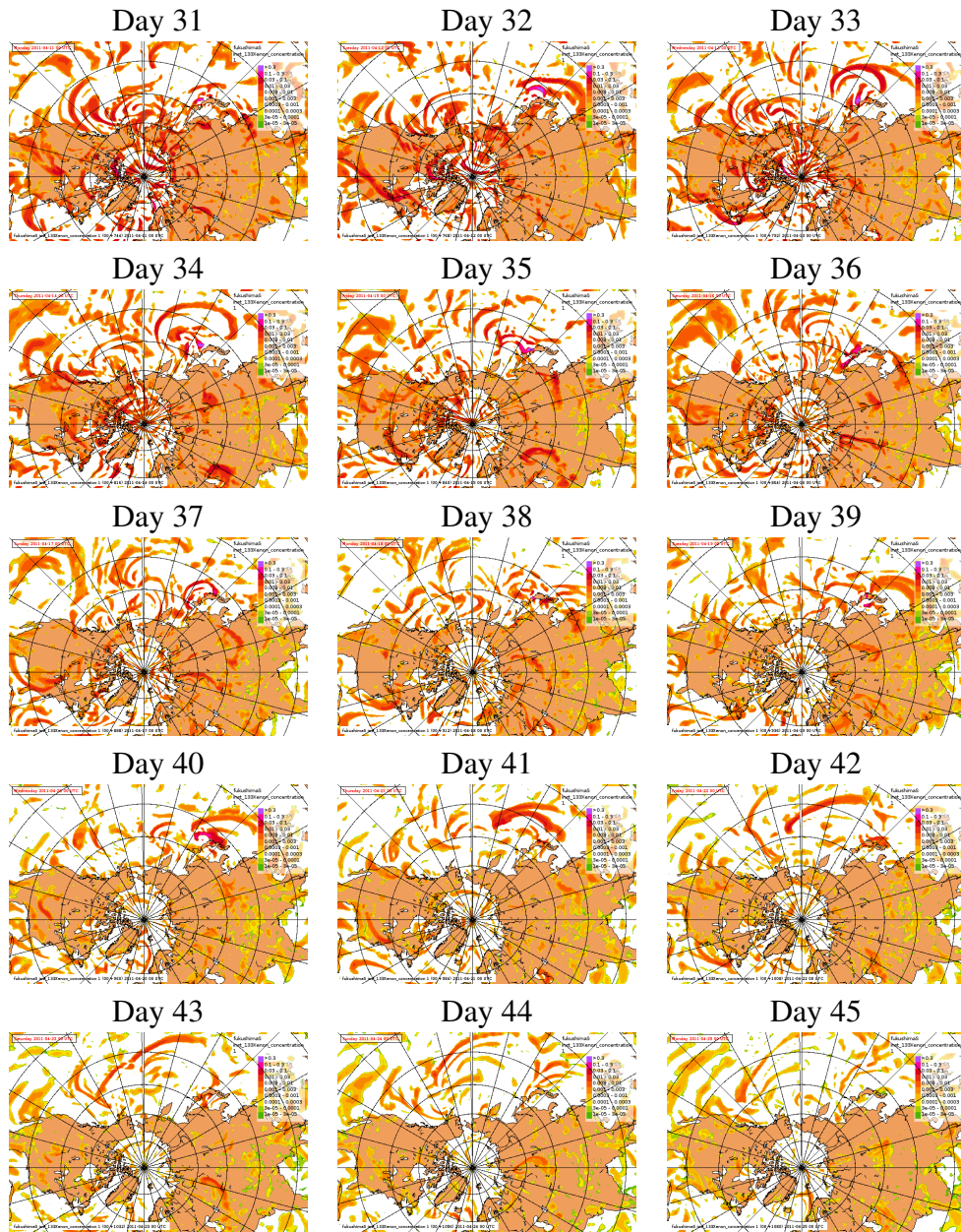
In this Appendix we show the results of the EEMEP model run with a long release - three months. The daily maps of instantaneous concentrations of Xe-133 and Cs-137 for the period of 92 days are presented. Units:  $\text{Bq m}^{-3}$ .

### Results for Xe-133. Days: 1-92



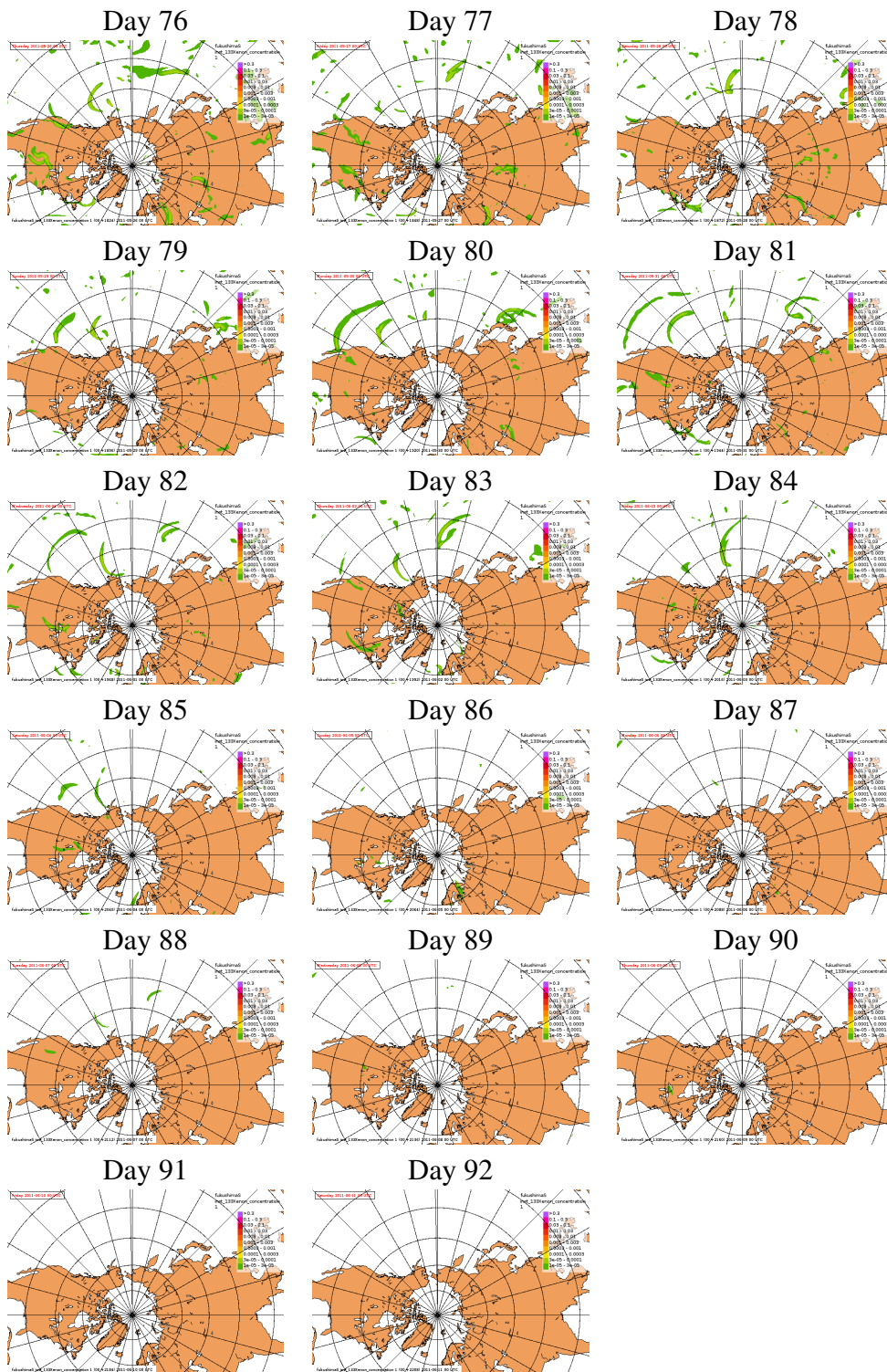


C. Daily results of EEMEP run with six weeks release



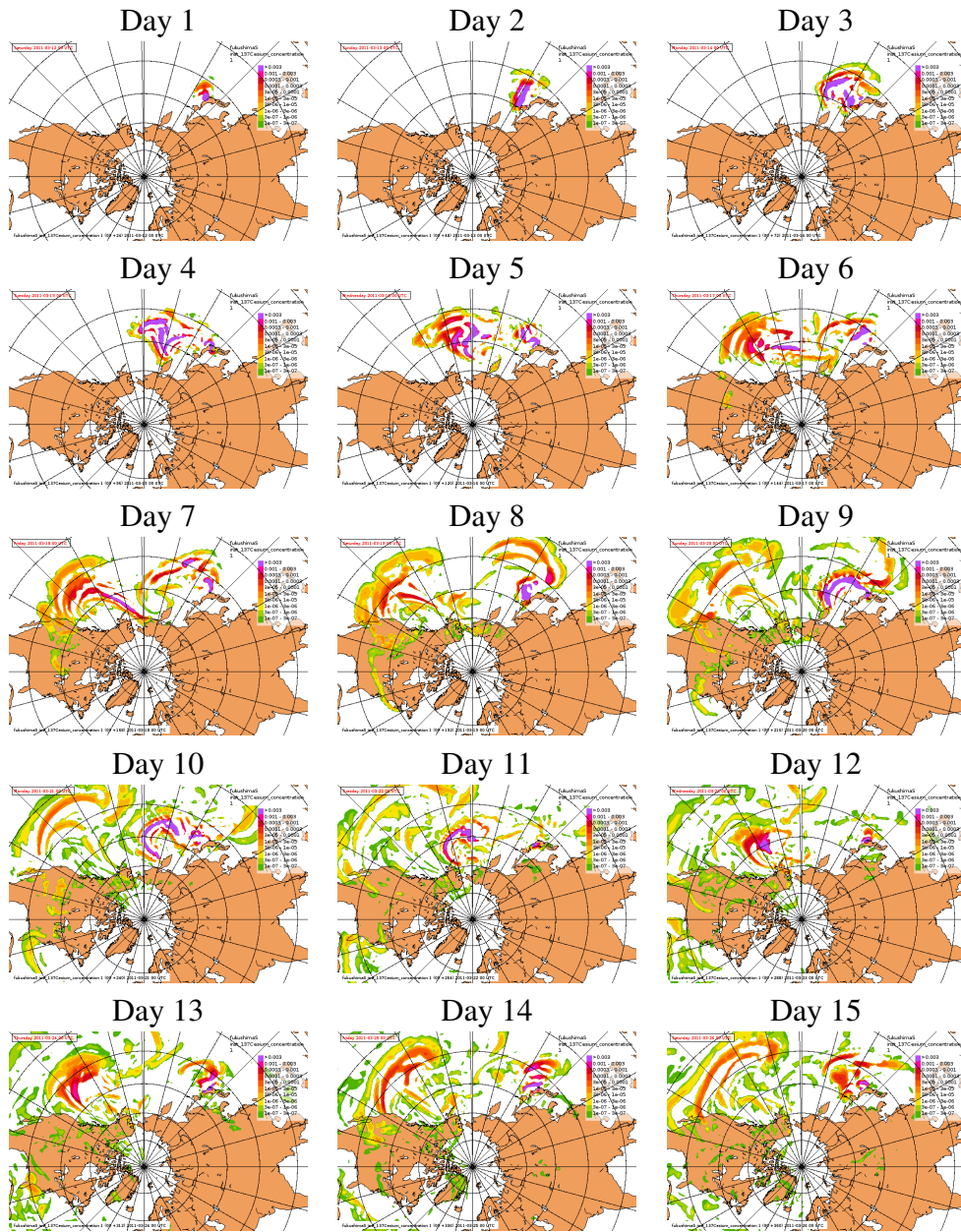




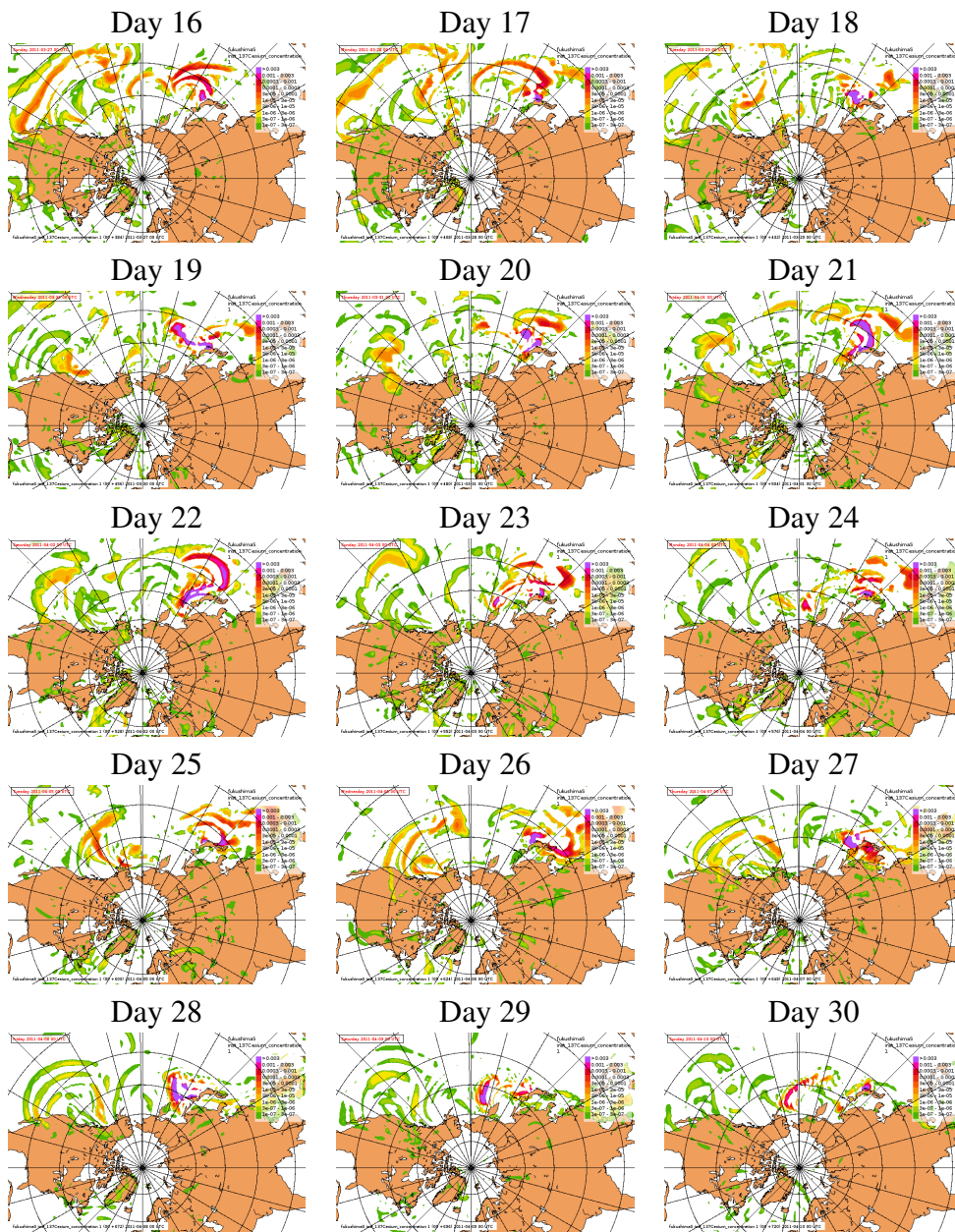


C. Daily results of EEMEP run with six weeks release

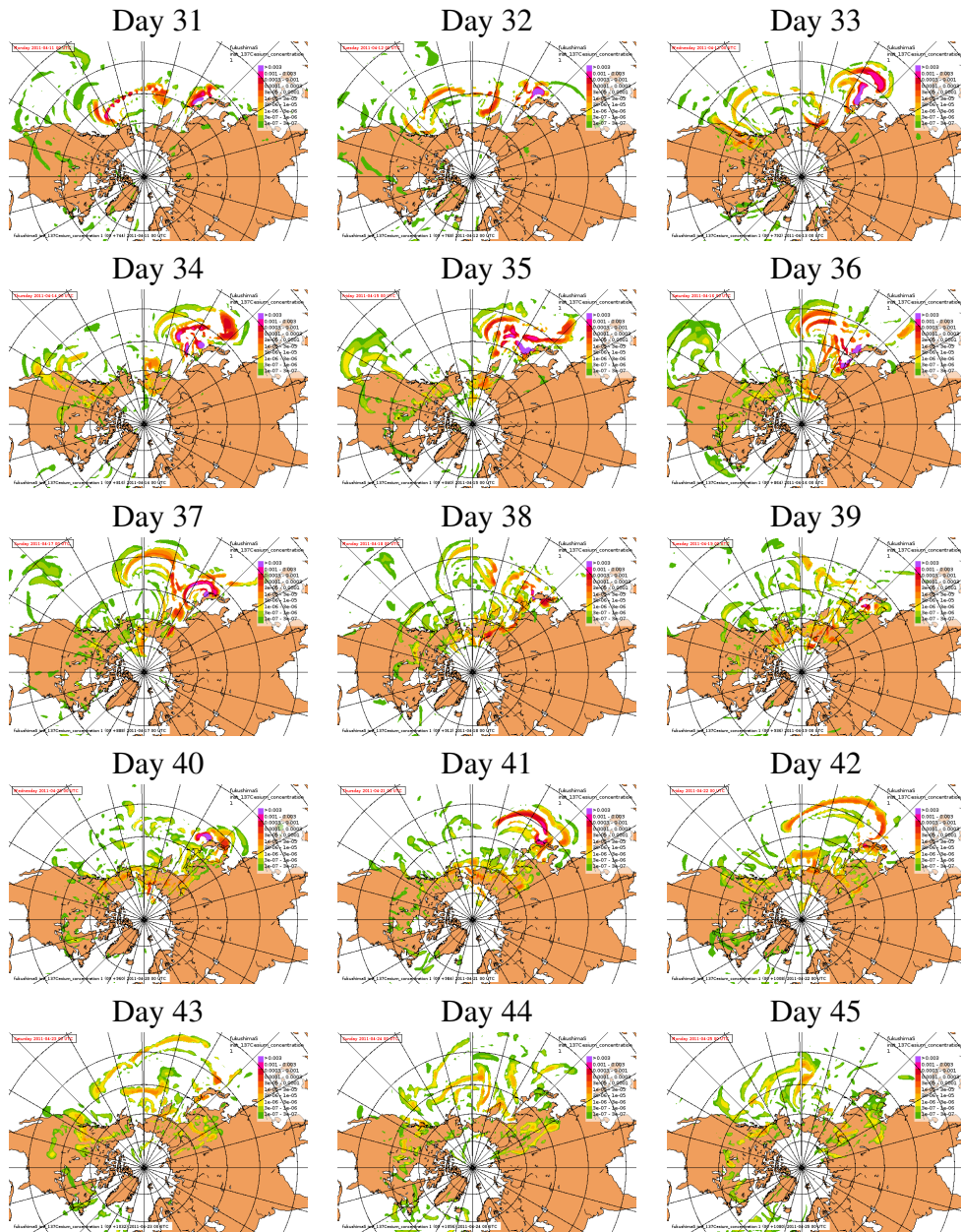
Results for Cs-137. Days: 1-92

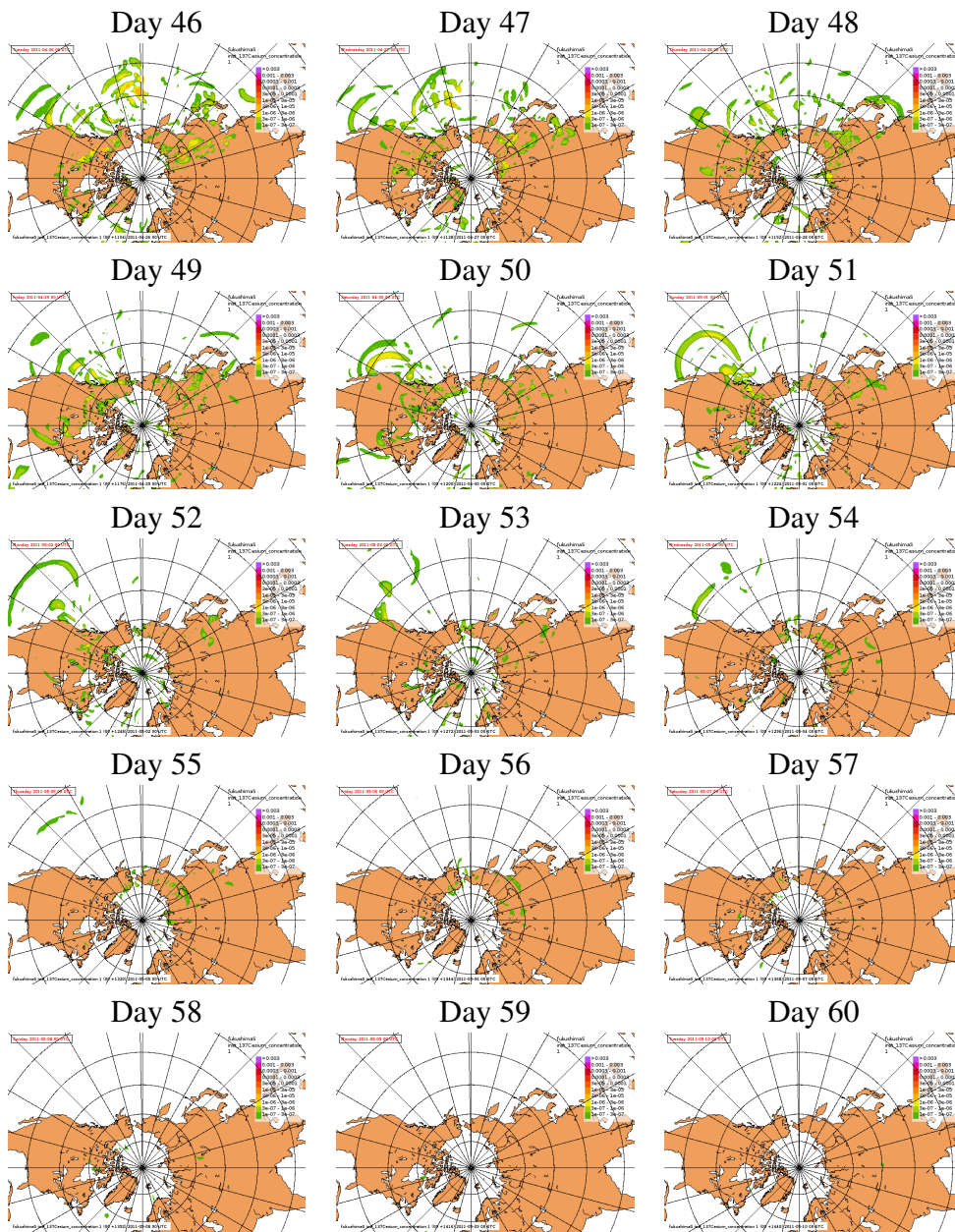






C. Daily results of EEMEP run with six weeks release





C. Daily results of EEMEP run with six weeks release

